Posttranslational modification of the RHO of plants protein RACB by phosphorylation and cross-kingdom conserved ubiquitination

Lukas Weiß[1], Tina Reiner[1], Julia Mergner[3], Bernhard Kuster[3,4], Attila Fehér[2], Götz Hensel[5], Manfred Gahrtz[5], Jochen Kumlehn[5], Stefan Engelhardt[1], Ralph Hückelhoven[1]*

*Corresponding author; mail: hueckelhoven@wzw.tum.de

Affiliations:

[1]Chair of Phytopathology, Technical University of Munich (TUM), Freising, Germany

[2]Chair of Plant Biology, University of Szeged, and Institute of Plant Biology, Biological Research Centre, Szeged, Hungary

[3]Chair of Proteomics and Bioanalytics, Technical University of Munich (TUM), Freising, Germany

[4]Bavarian Biomolecular Mass Spectrometry Center (BayBioMS), TUM, Freising, Germany

[5]Institute of Plant Genetics and Crop Plant Research (IPK), Gatersleben

Abstract:

Small RHO-type G-proteins act as signaling hubs and master regulators of polarity in eukaryotic cells. Their activity is tightly controlled, as defective RHO signaling leads to aberrant growth and developmental defects. Two major pathways regulate G-protein activity: canonical switching of the nucleotide bound state and posttranslational modification (PTM). PTMs can support or suppress RHO signaling, depending on each individual case. In plants, regulation of Rho of plants (ROPs) has been shown to act through nucleotide exchange and hydrolysis, as well as through lipid modification, but there is little data available on phosphorylation or ubiquitination of ROPs. Hence, we applied proteomic analyses to identify PTMs of the barley ROP RACB. We observed *in vitro* phosphorylation by barley ROP Binding Kinase 1 and *in vivo* ubiquitination of RACB. Comparative analyses of the newly identified RACB phosphosites and human RHO protein phosphosites revealed conservation of modified amino acid residues, but

no overlap of actual phosphorylation patterns. However, the identified RACB ubiquitination site is present in all ROPs from *Hordeum vulgare*, *Arabidopsis thaliana* and *Oryza sativa*. Since this highly conserved amino acid residue is likewise ubiquitinated in mammalian Rac1 and Rac3, we suggest that RHO family proteins from different kingdoms could be generally regulated by ubiquitination of this site.

Introduction:

Small guanosine triphosphate-binding (G-) proteins are master regulators of developmental and immunity-related processes. These include membrane transport, nuclear protein trafficking, reactive oxygen species production and cytoskeleton organization in growth and immunity (Irani et al., 1997; Lin and Yang, 1997; Jones et al., 2002; Yang, 2008; Ebine et al., 2011; Akamatsu et al., 2013). In humans (*Homo sapiens*, Hs), they are organized in the rat sarcoma (RAS) superfamily, comprised of the ARF, RAB, RAN, RAS and RHO families (Wennerberg et al., 2005), with the latter being further divided into Cdc42-like, Rho-like, RAC-like, RhoBTB and Rnd subfamilies (Lawson and Ridley, 2018). Plants however possess ARF, RAB and RAN family proteins, but only one type of small G-proteins from the RAS homologue (RHO) family, so called Rho of plants (ROPs). Traditionally, they were also called plant RACs (RAS-related C3 botulinum toxin substrate), due to their slightly higher similarity to metazoan RACs than RHO proteins. ROPs can be further distinguished based on their C-terminal hypervariable region and associated lipid modification. Type I ROPs can be reversibly *S*-acylated and additionally contain a CaaX-box motif that is a target for constitutive cysteine prenylation. Type II ROPs lack the CaaX-motif and are apparently constitutively *S*-acylated. Those cysteine lipid modifications are essential for plasma membrane anchoring and downstream signaling (Sorek et al., 2011; Yalovsky, 2015). Additionally, RHO proteins are often called molecular switches, as they cycle between a guanosine diphosphate (GDP)-bound “OFF” state and guanosine triphosphate (GTP)-bound “ON” state. The nucleotide cycling itself is tightly controlled by a set of specific proteins: guanosine nucleotide exchange factors (GEFs) facilitate the GDP to GTP exchange, which leads to G-protein activation. In turn, GTPase

53 activating proteins (GAPs) target GTP-bound G-proteins and stimulate their weak intrinsic
54 GTPase activity to hydrolyse GTP to GDP to turn them “OFF” again (Berken and Wittinghofer,
55 2008). This nucleotide exchange is accompanied by a conformational shift, which affects
56 interaction with other proteins (Milburn et al., 1990; Berken, 2006). A third class of regulatory
57 proteins, so-called guanine nucleotide dissociation inhibitors (GDIs), target mostly the
58 GDP-bound state and recruit the G-protein to the cytoplasm, blocking it from downstream
59 signaling (Boulter and Garcia-Mata, 2010).

60 Lipidations are not the only posttranslational modifications (PTM) in RHO proteins. In animals
61 both phosphorylation and ubiquitination are employed to control RHO signaling, thereby
62 enhancing or suppressing G-protein function in a case-dependent manner. The mammalian
63 RHO family member Rac1 for instance is phosphorylated at three amino acids by different
64 kinases: focal adhesion kinase (FAK) and proto-oncogene tyrosine-protein kinase Src (cellular
65 sarcoma) phosphorylate Rac1 *in vitro* at Y64 (Chang et al., 2011). Phosphomimetic
66 Rac1-Y64D mutants showed decreased GTP-binding and association with downstream
67 signaling proteins, and cells expressing Rac1-Y64D displayed defects in focal adhesion
68 targeting and cell spreading. Extracellular signal-related kinase (ERK) phosphorylates Rac1 at
69 T108, targeting it to the nucleus before prenylation and hence isolating it from activation by
70 cytosolic GEFs (Tong et al., 2013). Phosphorylation of Rac1 by the AGC kinase AKT (RAC-
71 alpha serine/threonine-protein kinase 1) at S71 has been shown to be essential for targeting
72 by an F-box/Leucine-rich repeat (FBXL) protein (Kwon et al., 2000; Zhao et al., 2013). F-box
73 proteins are part of SKP1-CUL1-F-box (SCF) E3 ubiquitin ligase complexes which mediate
74 ubiquitination and proteasomal degradation of selected proteins (Hua and Vierstra, 2011).
75 SCF^{FBXL19} targets S71-phosphorylated Rac1, which leads to ubiquitination of Rac1 K166 (Zhao
76 et al., 2013). This depletes Rac1 from cells, which inhibits its function in cell spreading. Another
77 Rac1 ubiquitination site is K147, which is targeted by HECT domain and ankyrin repeat
78 containing E3 ubiquitin protein ligase 1 (HACE1) and two inhibitor of apoptosis proteins (IAPs).
79 While HACE1 mainly targeted GTP-bound Rac1, both XIAP and c-IAP1 did not show any
80 preference for a particular nucleotide-bound state. In all cases, ubiquitination of K147 leads to

81 proteasomal degradation of Rac1, abolishing its function in cell migration (Torrino et al., 2011;
82 Oberoi et al., 2012; Castillo-Lluva et al., 2013). For mammalian RhoA, four phosphorylation
83 sites and three ubiquitination sites have been identified. Phosphorylation of S26 by mammalian
84 Sterile20-related kinase 3 (Mst3) leads to increased intrinsic GTPase activity of RhoA and
85 associated depolymerization of F-actin, which is necessary for proper neuron positioning in the
86 developing mouse brain (Tang et al., 2014). ERK phosphorylates RhoA at S88 and T100,
87 enhancing GTP-binding and actin stress fiber formation in mammalian cell lines (Tong et al.,
88 2016). In contrast, protein kinase A (PKA)-mediated phosphorylation of S188 results in eviction
89 of RhoA from the plasma membrane with the help of RhoGDI, impeding RhoA function and
90 protecting it from ubiquitin-mediated degradation (Lang et al., 1996; Forget et al., 2002;
91 Ellerbroek et al., 2003; Rolli-Derkinderen et al., 2005). Ubiquitination of RhoA has also been
92 demonstrated, with K6 and K7 being targets of Smad ubiquitylation regulatory factor 1
93 (Smurf1), while K135 is ubiquitinated by SCF^{FBXL19}. These modifications resulted in a loss of
94 tight junctions in epithelial cells and suppressed RhoA-mediated cytoskeleton organization and
95 cell proliferation, respectively (Ozdamar et al., 2005; Wei et al., 2013) (for an overview of Rac1
96 and RhoA PTMs, see Supplemental Figure 1).

97 Compared to the mammalian field, knowledge about phosphorylation and ubiquitination in
98 ROPs is limited. To date, phosphorylation of *Arabidopsis thaliana* (At) ROP4 and ROP6 by
99 ROP BINDING PROTEIN KINASE 1 (RBK1), a receptor-like cytoplasmic kinase (RLCK) of
100 class VI_A, has been shown. RBK1 interacts with Mitogen-activated protein kinase 1 (MPK1)
101 of an auxin-responsive MPK cascade, indicating that regulation of ROP4 and ROP6 via
102 phosphorylation might be important for auxin-dependent cell expansion (Enders et al., 2017).
103 Furthermore, type II AtROP10 and AtROP11 are phosphorylated at S138, but no functional
104 studies about these phosphosites have been conducted yet (Mergner et al., 2020). Introduction
105 of a phosphomimetic S-to-E mutation of the broadly conserved S74 in AtROP4 and *Medicago*
106 *sativa* MsROP6 has been investigated. The S74E mutation did not alter GTPase activity, but
107 blocked interaction with an upstream activating ROPGEF, weakened binding to a downstream

108 signaling kinase and showed lesser *in vitro* kinase activation (Fodor-Dunai et al., 2011).
109 However, evidence for *in vivo* phosphorylation of type I ROPs is lacking.

110 In barley (*Hordeum vulgare, Hv*), ROPs have been investigated in the interaction between
111 barley and the powdery mildew fungus *Blumeria graminis* f.sp. *hordei* (*Bgh*). There, it was
112 shown that most barley ROPs are supporting the penetration success of *Bgh* (Schultheiss et
113 al., 2002; Schultheiss et al., 2003; Pathuri et al., 2008; Hoefle et al., 2011). Among these
114 ROPs, RACB is the best characterized ROP family member. Under physiological conditions,
115 it is required for root hair outgrowth and stomatal subsidiary cell formation. RACB and its
116 interacting proteins further steer cytoskeleton organization (Opalski et al., 2005; Pathuri et al.,
117 2008; Pathuri et al., 2009; Scheler et al., 2016). During *Bgh* attack, however, it was shown that
118 RNA-interference (RNAi)-mediated knockdown of RACB decreased the penetration success
119 of the fungus into barley epidermal cells, whereas overexpression of constitutively activated
120 RACB (CA, RACB-G15V) promoted susceptibility (Schultheiss et al., 2002; Schultheiss et al.,
121 2003; Pathuri et al., 2008; Hoefle et al., 2011). In contrast, transient overexpression of neither
122 wildtype (WT) nor dominant negative RACB (DN, RACB-T20N) increased barley susceptibility,
123 indicating that the GTP-bound, active form of RACB supports fungal invasion into intact barley
124 cells.

125 Since RHO family proteins interact with several downstream effectors in order to perform their
126 function in signaling, interaction partners of RACB were investigated with regard to barley
127 susceptibility to *Bgh*. It was shown that two classes of scaffolding proteins, ROP-interactive
128 partners (RIPs) and ROP-interactive and CRIB-domain containing proteins (RICs), associate
129 with CA-RACB at the plasma membrane and enhance penetration success of *Bgh* into barley
130 epidermal cells when overexpressed (Schultheiss et al., 2008; Engelhardt et al., 2019;
131 McCollum et al., 2019). In contrast, two other RACB protein-protein interaction partners
132 support resistance to fungal penetration. MICROTUBULE-ASSOCIATED GTPASE
133 ACTIVATING PROTEIN 1 (MAGAP1) enhances resistance towards *Bgh* and likely regulates
134 RACB by supporting GTP hydrolysis (Hoefle et al., 2011). Barley RBK1 interacts with

135 CA-RACB in yeast and *in planta*, and CA-RACB increases RBK1 kinase activity *in vitro*. RBK1
136 may be a RACB effector kinase, since co-expression of CA-RACB and RBK1 results in
137 co-localization of both proteins at the plant plasma membrane via recruitment of the otherwise
138 cytosolic RBK1. However, opposite to the effect for RACB, transient knockdown of RBK1
139 results in increased disease susceptibility and reduced microtubule stability (Huesmann et al.,
140 2012). Another protein-protein interaction partner of RBK1, S-PHASE KINASE 1-
141 ASSOCIATED PROTEIN-LIKE (SKP1L), is also involved in resistance towards *Bgh* (Reiner et
142 al., 2016). SKP1L may be a subunit of an SCF E3 ubiquitin ligase complex, which targets
143 specific proteins for polyubiquitination and proteasomal degradation (Hua and Vierstra, 2011).
144 In line with this predicted function, it was demonstrated that RBK1, SKP1L and the 26S
145 proteasome negatively influence protein abundance of CA-RACB, presumably acting in a
146 negative feedback-loop towards the ROP (Reiner et al., 2016).

147 In this study, we confirm that kinase activity of RBK1 is strongly enhanced in the presence of
148 CA-RACB. This results in phosphorylation of both RBK1 and CA-RACB *in vitro*. Phosphosite
149 mapping revealed novel phosphorylated residues in RACB that were not previously described
150 to be modified in other RHO family proteins. We further found that CA-RACB shows an
151 ubiquitination-typical appearance of high molecular weight derivatives after proteasome
152 inhibition. Mass spectrometry revealed that CA-RACB is ubiquitinated in barley at K167, a
153 residue which is conserved in mammalian Rac1, Rac3 and all other ROPs of barley, rice and
154 Arabidopsis.

155

156 **Results**

157 **CA-RACB is phosphorylated by RBK1 *in vitro***

158 In a previous study, we showed that constitutively activated (CA-) RACB interacts with RBK1
159 *in vivo* and enhances its kinase activity *in vitro* (Huesmann et al., 2012). To test, if RACB is
160 phosphorylated during this protein-protein interaction, we carried out an *in vitro* radiolabeling
161 kinase assay with recombinant His-tagged RBK1 and CA-RACB (see Fig. 1A). For His-tagged
162 *Medicago sativa* MsROP6, Dorjgotov et al. (2009) showed that RBK1-like RLCK VI_A kinases
163 phosphorylate the His-tag and linker, but not the ROP protein itself *in vitro*. We hence designed
164 the cloning strategy in a way that avoids creation of potential artificial phosphorylation sites,
165 which could otherwise be formed. Since RBK1 shows some constitutive kinase activity *in vitro*
166 (Huesmann et al., 2012), we used low RBK1 protein amounts in this assay. RBK1 alone
167 displayed only weak autophosphorylation activity under these conditions. In the presence of
168 CA-RACB, we then observed strong phosphorylation of both CA-RACB and RBK1. No
169 phosphorylation could be detected after incubation with a RBK1 kinase-dead mutant (KD,
170 K245D, also see Fig. 1B for RBK1 protein stability) or in a water-control reaction.

171 To identify phosphosites in RACB, we conducted the *in vitro* kinase assay using unlabeled
172 ATP and detected *in vitro* phosphosites of CA-RACB via mass spectrometry (see Fig. 2A).
173 This revealed high confidence CA-RACB peptides with phosphorylated residues at positions
174 S97, T139, S159, S160 and T162. Since in the case of the neighboring serines S159 and S160
175 the localization of the phospho-modification could not be specifically assigned within the
176 peptide sequence (see Supplemental Table 1), both residues were treated as possible but
177 alternative phosphosites. Using computational modelling of the RACB protein structure based
178 on the protein models of GDP-bound AtROP4 and GTP-analog-bound HsRAC1, we suggest
179 that S97, T139 and T162 are surface-exposed in RACB, whereas this is less clear for S159
180 and S160 (see Fig. 2B).

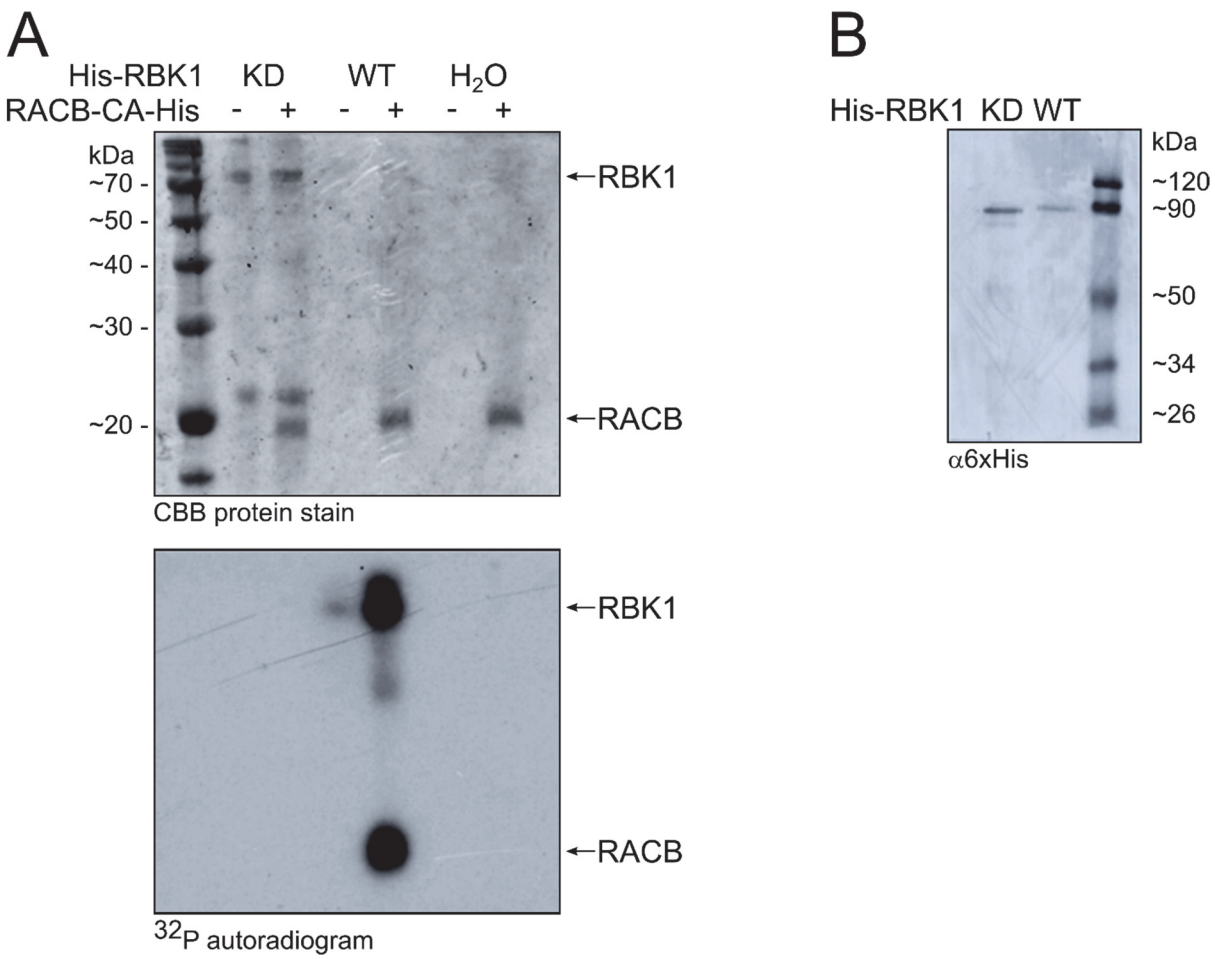

Figure 1: *In vitro* co-incubation of RACB and RBK1 results in phosphorylation of both proteins.

A: Low amounts of His-tagged RBK1 alone show weak autophosphorylation *in vitro*. Kinase activity is enhanced by the presence of constitutively activated His-tagged CA-RACB, resulting in extensive phosphorylation of both proteins. Upper panel = protein loading control. Lower panel = autoradiogram showing ^{32}P-labelled, phosphorylated proteins. WT = wildtype RBK1; KD = kinase-dead RBK1 loss-of-function mutant (K245D); H_2O = no kinase control. Estimations of molecular weight are depicted in kilo Dalton (kDa) on the left.

B: Western blot showing stability of both WT and KD His-RBK1.

We also tried to map *in vivo* phosphorylation sites for RACB. To this end, we made use of transgenic barley lines overexpressing HA-tagged full-length CA-RACB, a cytosolic

194 non prenylated CA-RACB-ΔCSIL mutant (Schultheiss et al., 2003) or the HA-tag alone.
195 Initially, we generated 47 transgenic plants for HA-CA-RACB, 37 plants for HA-RACB-ΔCSIL
196 and 40 plants for HA alone. We propagated these lines and selected the offspring using PCR,
197 resistance against hygromycin and Western blotting (not shown). Thereby, we could see that
198 all positive plants expressed the expected HA-tagged proteins, except for the free HA-tag,
199 which could not be detected on a Western blot, most likely because the peptide is too small
200 (see Fig. 3A). We further analyzed three transgenic plants of one line per construct with regard
201 to susceptibility towards powdery mildew. Upon infection with *Bgh*, plants overexpressing full-
202 length CA-RACB displayed increased disease susceptibility compared to the free HA-control,
203 whereas the CA-RACB-ΔCSIL mutants did not show an altered disease phenotype (see Fig.
204 3B).

205 From the transgenic HA-CA-RACB overexpressing plants, we initially isolated protoplasts and
206 treated them with the proteasome inhibitor MG132 before protein extraction. We enriched
207 HA-tagged CA-RACB using immunoprecipitation, digested proteins with trypsin and selected
208 for phosphorylated peptides using Immobilized Metal Affinity Chromatography (IMAC).
209 Peptides and posttranslational modifications were identified via mass spectrometry, but did not
210 indicate CA-RACB phosphosites (not shown). In the following experiment, we co-expressed
211 RBK1 in transgenic protoplasts before MG132 treatment, and selectively skipped
212 immunoprecipitation or IMAC (see Supplemental Figure 2A). However, we were repeatedly
213 unsuccessful in identifying *in vivo* phosphopeptides of RACB (see Supplemental Table 2). In
214 a third approach, we tried to map RACB phosphorylation after transient co-expression of RBK1
215 and proteasome inhibition by MG132 in transgenic HA-CA-RACB overexpressing barley
216 protoplasts. From this, we extracted proteins, performed a tryptic digest and enriched
217 phosphopeptides via IMAC. These samples were subsequently decomplexed by high pH
218 reversed-phase fractionation to increase the discovery rate of peptides during mass
219 spectrometry. This identified more than 5,000 phosphopeptides from diverse barley proteins,
220 including ROP signaling components such as three different barley ROPGAPs, thus providing
221 a resource for the barley research community. Because our experimental design included *in*

222 *vivo* expression of combined or single GFP-tagged RBK1 and HA-CA-RACB (Supplemental
223 Figure 2B), some of the mapped barley phosphosites might be CA-RACB- and/or RBK1-
224 dependent (see Supplemental Table 3). Therefore, this needs further analysis. Despite the
225 high amount of identified phosphopeptides, no *in vivo* phosphopeptides of CA-RACB were
226 recovered.

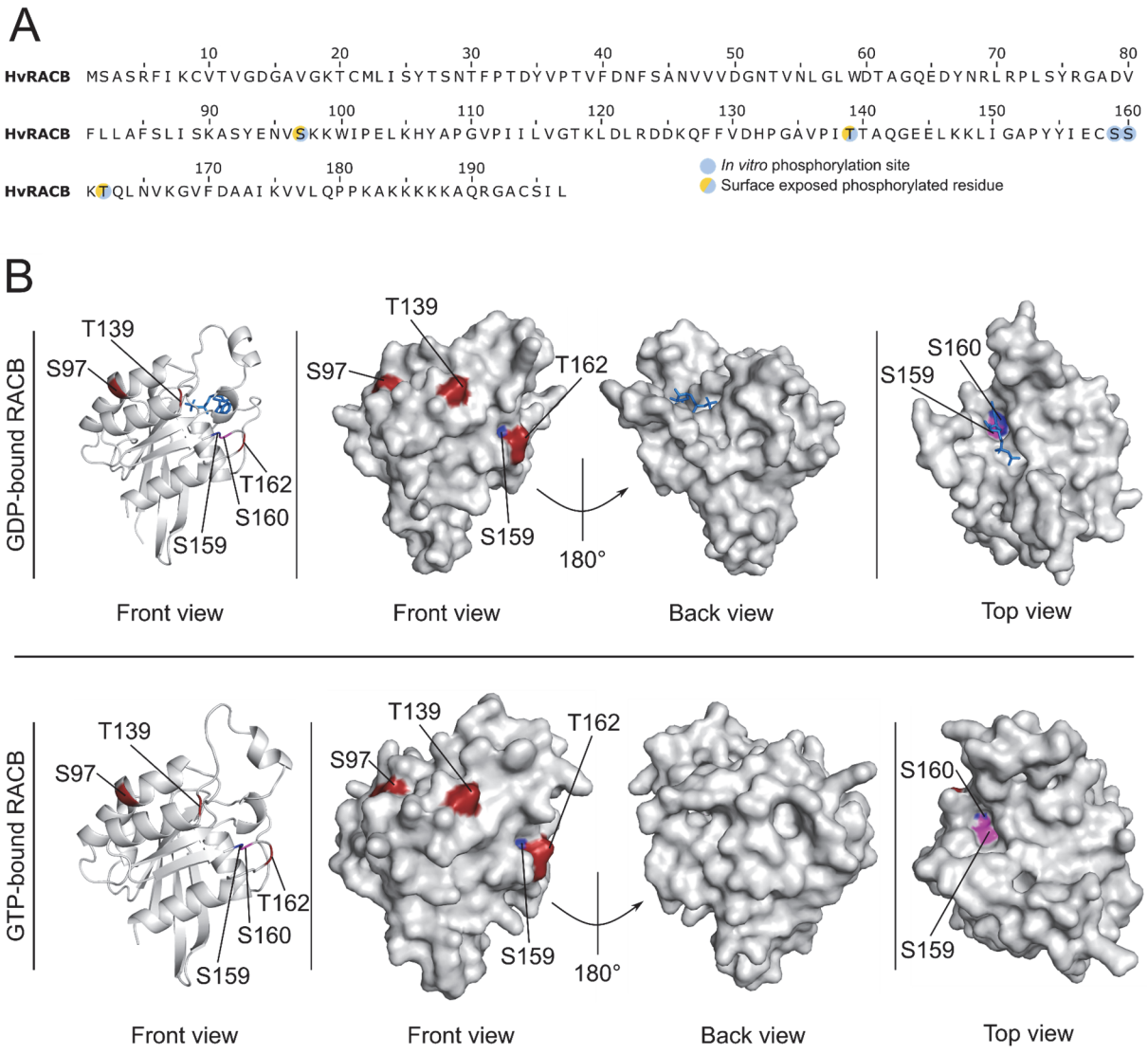

227
228

229 **Figure 2: Surface-exposure of CA-RACB *in vitro* phosphosites.**

230 **A:** Phosphorylation sites of CA-RACB are shown in blue, predicted surface-exposed residues
231 are additionally highlighted in yellow. *In vitro* phosphorylation sites of RACB were identified by
232 mass spectrometry after *in vitro* co-incubation of CA-RACB and RBK1.

233 **B:** Upper panel: the model of GDP-bound WT RACB (amino acids 1-178 from 197 total) was
234 built with GDP-bound AtROP4 as template (PDB entry: 2NTY.1 (Thomas et al., 2007)). Lower
235 panel: GTP-bound WT RACB (amino acids 7-178 from 197 total) was modelled using HsRAC1
236 associated with GNP (phosphoaminophosphonic acid-guanylate ester, a non-hydrolysable
237 GTP-analog) as template (PDB entry: 3TH5.1 (Krauthammer et al., 2012)). Phosphorylated
238 surface-exposed residues are shown in red, GDP as ligand in blue. Only S97, T139 and T162
239 are surface-exposed, S159 (pink) and S160 (blue) are not clearly exposed to the surface.
240 Putative RACB folds were assembled by homology-modelling using SWISS-MODEL
241 (Waterhouse et al., 2018). Surface structure (front, back and top view) and cartoon (front view)
242 illustrations were modelled in PyMOL (Schrodinger, 2015).

243

244 Although we primarily aimed at identifying phosphopeptides of RACB, our datasets were
245 equally suitable for mapping phosphosites in RBK1 (see Fig. 4). In the *in vitro* kinase assay,
246 we found RBK1 to be phosphorylated at positions S26, S30, S98, S100, S107, T110, S155,
247 T170 and S436. In the two experiments involving *in vivo* co-overexpression of CA-RACB and
248 RBK1 (see Supplemental Figure 2A and Figure 4B), we found RBK1 phosphosites at positions
249 S26, S30, S160, T170, S189, S197, S518, T521 and S26, S30, S100, S107, S113, S114,
250 S216, T525, respectively. Overlapping sites from *in vitro* and at least one *in vivo* experiment
251 are therefore S26, S30, S100, S107 and T170.

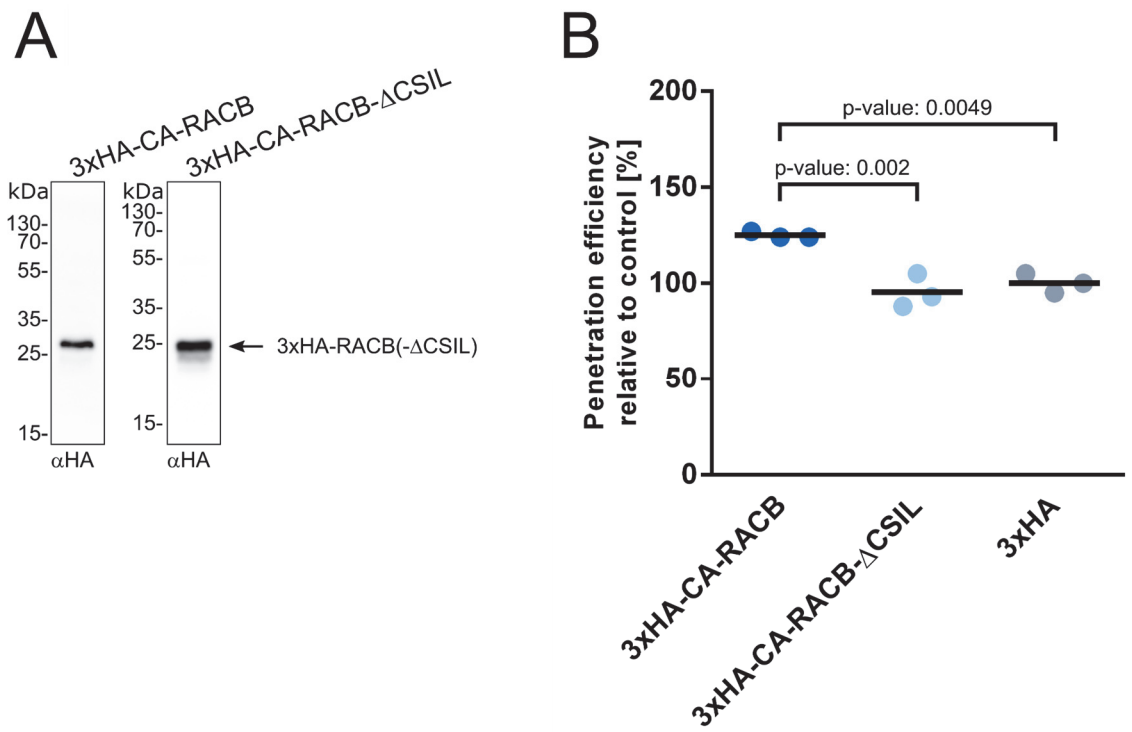

Figure 3: Transgenic barley plants overexpressing HA-tagged CA-RACB show increased *Bgh* susceptibility.

A: Both HA-tagged full-length CA-RACB and CA-RACB-ΔCSIL are stably expressed in transgenic barley.

B: Transgenic plants expressing full-length HA-tagged CA-RACB are more susceptible towards penetration by *Bgh*, while plants expressing the truncated CA-RACB-ΔCSIL mutant show the same level of susceptibility as the HA-control. For each construct, three plants of one transgenic line were tested. Each datapoint corresponds to one plant. Statistical significances were determined using a One-way ANOVA with Tukey's HSD.

A

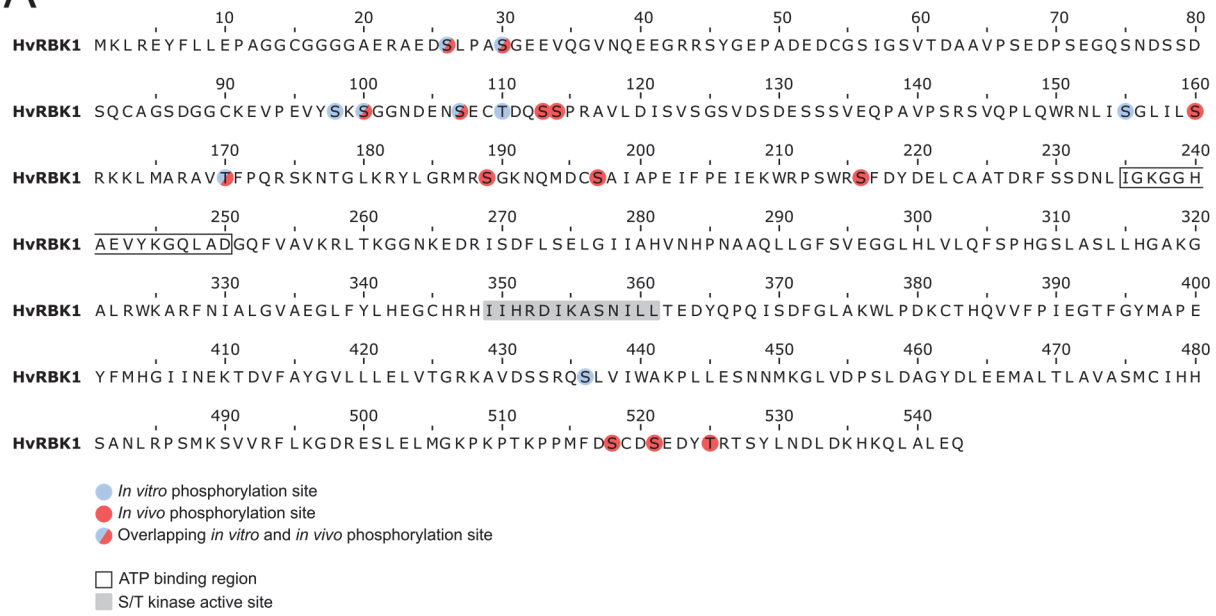

B

In vitro sites	*In vivo* sites experiment 1	*In vivo* sites experiment 2
S26	S26	S26
S30	S30	S30
S98	-	-
S100	-	S100
S107	-	S107
T110	-	-
-	-	S113
-	-	S114
S155	-	-
-	S160	-
T170	T170	-
-	S189	-
-	S197	-
-	-	S216
S436	-	-
-	S518	-
-	S521	-
-	-	T525

Figure 4: Comparison between *in vitro* and *in vivo* RBK1 phosphosites.

A: Barley RBK1 sequence with marked *in vitro* (blue) and *in vivo* (red) phosphosites. Residues phosphorylated under both conditions are shown in half circles of blue and red. *In vitro* phosphorylated amino acids were identified in an *in vitro* kinase assay, in which His-tagged RBK1 and His-tagged CA-RACB were co-incubated. *In vivo* phosphosites were found in transgenic HA-CA-RACB overexpressing protoplasts in the presence of transiently co-expressed GFP-tagged RBK1 and the proteasome-inhibitor MG132. Phosphopeptides were enriched from total protein extracts of protoplast lysates using IMAC (experiment 1) and additionally decomplexed by high pH reversed-phase fractionation (experiment 2). All *in vitro* and *in vivo* phosphosites were identified by mass spectrometry.

B: List of RBK1 phosphosites from all *in vitro* and *in vivo* experiments.

274 **CA-RACB is ubiquitinated *in vivo***

275 Previously, we found that the protein abundance of CA-RACB is negatively influenced by
276 RBK1, SKP1L and the proteasome (Reiner et al., 2016). For this reason, we investigated if we
277 could detect ubiquitination of CA-RACB *in vivo*. We used MG132 for proteasome inhibition in
278 primary leaves of transgenic barley overexpressing HA-tagged CA-RACB. This led to detection
279 of HA-CA-RACB and higher molecular weight derivatives on Western blots after
280 αHA-immunoprecipitation and detection via anti-HA antibodies (see Fig. 5A). As this laddering
281 is a potential indicator for ubiquitination of a target protein (Gohre et al., 2008; Lu et al., 2011),
282 we attempted to map the residue(s) at which RACB might be ubiquitinated. We first conducted
283 a global mass spectrometry analysis, in which we specifically looked for branched amino acid
284 sequences as derived from ubiquitinated lysine residues after tryptic digest (see Supplemental
285 Figure 2C). Interestingly, we found the peptide containing RACB K167 carrying a mass shift
286 equal to 2 glycine molecules (see Fig. 5B). This mass shift indicates that K167 is indeed
287 ubiquitinated, as two glycine residues typically remain at ubiquitinated lysine residues
288 (glyglycylation), whereas the rest of the ubiquitin moiety is cleaved by trypsin during sample
289 digestion (Peng et al., 2003). Evidence for RACB ubiquitination was subsequently
290 substantiated in a targeted parallel reaction monitoring (PRM) approach. Comparison with
291 other ROPs from barley, rice and Arabidopsis showed that RACB K167 is a highly conserved
292 residue in ROPs (see Fig. 6 and Supplemental Figure 3).

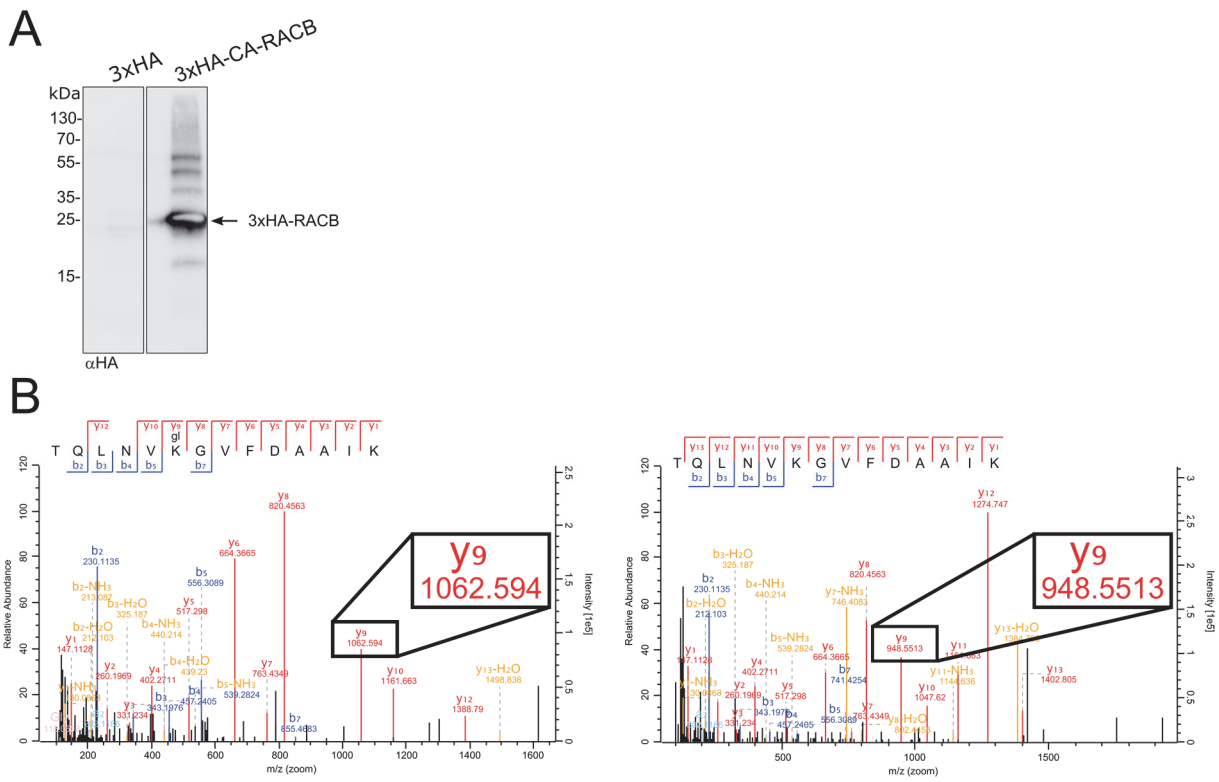

Figure 5: Constitutively activated RACB is ubiquitinated *in vivo*.

A: HA-tagged CA-RACB and higher molecular weight bands were detected in an αHA-Western blot after MG132 treatment and αHA-immunoprecipitation from whole barley leaves stably expressing 3xHA or 3xHA-CA-RACB (see Fig. S2B).

B: Ubiquitination of CA-RACB at K167 was identified by mass spectrometry in a workflow described in Fig. S2B. The left graph shows spectra of the recovered ubiquitinated peptide, while the right graph shows the corresponding unmodified peptide. The black box illustrates one example: fragment "y9" was recovered with two different masses. The difference corresponds to that of 2 glycines, which is typical after a tryptic digest of ubiquitinated proteins (Peng et al., 2003). Example: $y9_{modified}$ (1062.59 m/z) – $y9_{unmodified}$ (948.55 m/z) = 114.04 m/z = 2 * glycine (57.02 m/z).

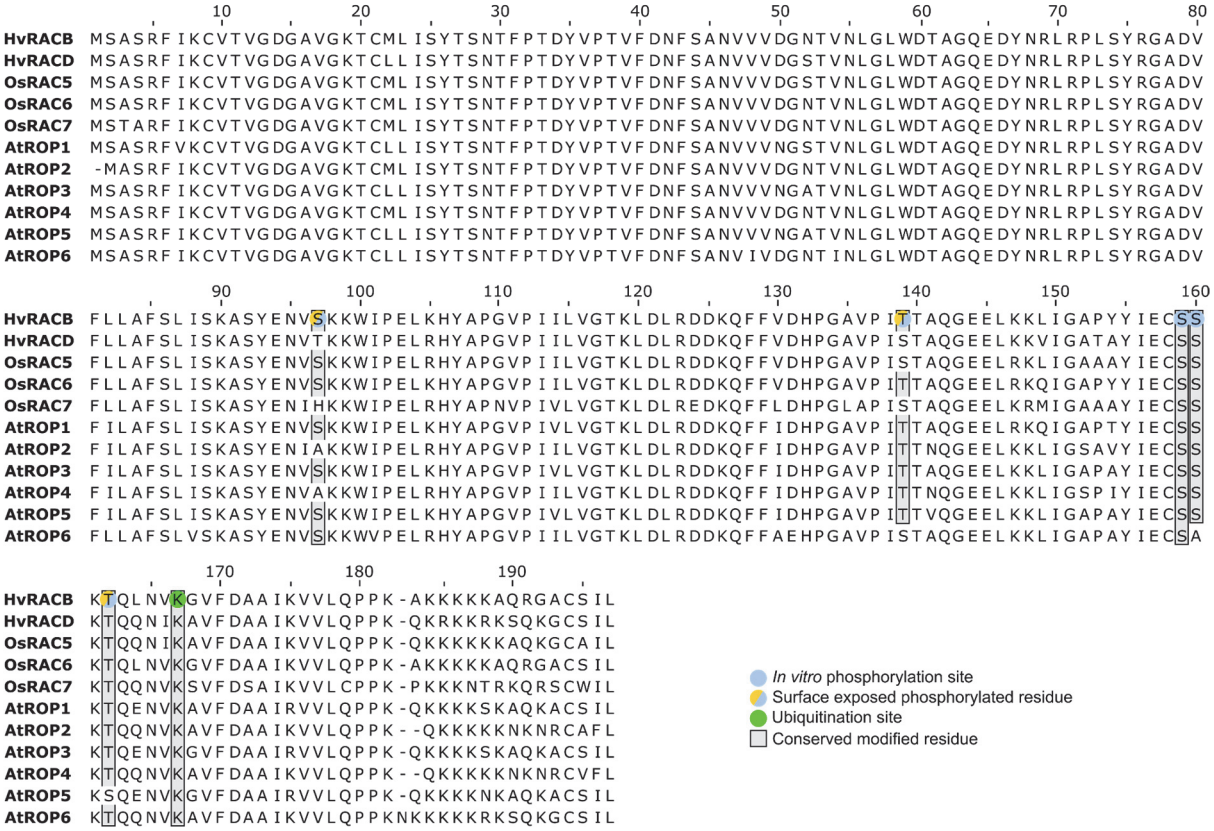

Figure 6: Alignment of type I ROPs from barley (*Hordeum vulgare*, *Hv*), rice (*Oryza sativa, Os*) and *Arabidopsis thaliana* (*At*).

The ubiquitinated residue from CA-RACB (K167, green) is conserved across all type I ROPs from the three species (shaded box). *In vitro* phosphosites of RACB (blue) are conserved among some type I ROPs (shaded box). Surface-exposed phosphosites are additionally highlighted in yellow.

Discussion

Small RHO family proteins are signaling hubs and master regulators of cell polarity. Their function is tightly regulated, for instance by PTMs. Lipid modifications, phosphorylation and ubiquitination have been well described in the recent years, which can have an activity-enhancing or suppressing influence on the RHO protein, depending on each individual case. Other PTMs, such as glycosylation and adenylylation have been described, but they are

322 predominantly employed by pathogens which target RHO family proteins via virulence
323 effectors (Worby et al., 2009; Jank et al., 2013).

324 In plants, ROP regulation by GEFs and GAPs has been shown (Wu et al., 2000; Berken et al.,
325 2005; Klahre and Kost, 2006; Hoefle et al., 2011; Akamatsu et al., 2013), but there is little data
326 available on posttranslational regulation of ROPs beyond prenylation and *S*-acylation. In this
327 study, we show *in vitro* phosphorylation and *in vivo* ubiquitination of the barley ROP RACB.
328 S97, T139 and T162 *in vitro* phosphosites are predicted to be surface-exposed and therefore
329 could be also targets for RBK1-dependent phosphorylation of RACB *in vivo* (see Fig. 2). This
330 is less clear for S159 and S160. Nevertheless, one can speculate that they could become
331 accessible *in vivo* after other posttranslational modification of RACB, which cause a
332 conformational shift in the RACB structure. It would be furthermore possible that
333 phosphorylation of S159/S160 interferes with RACB signaling, since these residues are in
334 direct proximity of the putative *S*-acylation site C158 and the nucleotide binding pocket (see
335 Fig. 2 and Supplemental Figure 1; Sorek et al. (2010); Sorek et al. (2017)). However, this
336 remains hypothetical, as we did not find evidence for *in vivo* phosphorylation of these amino
337 acids. All five phosphorylated residues are partially conserved in other type I and type II ROPs,
338 indicating that these sites might be common targets for phosphorylation of RBK1-like RLCK
339 VI_A kinases in plants. The only known *in vivo* ROP phosphosite, S138 from AtROP10 and
340 AtROP11 (see Supplemental Figure 3; Mergner et al. (2020)), is not conserved in RACB, which
341 indicates that this might be a type II ROP-specific modification site. In any case, introducing
342 point mutations at these sites could help answering, which role they play in regulating ROP
343 function.

344 Comparison of RACB phosphosites with those of mammalian Rac1 and RhoA revealed that
345 there is no overlap between mapped animal and plant phosphosites, although several modified
346 residues are conserved across kingdoms (see Supplemental Figure 1). Thus, it is well possible
347 that RACB is also phosphorylated at Y67, S74 and S89 by other kinases, but in our *in vitro*
348 and *in vivo* approaches we did not identify modification of these residues. Still, conservation of

349 these amino acids suggests that RACB could be regulated in a similar fashion as mammalian
350 RHO family proteins. Interestingly, phosphorylation of these residues in mammalian RHO
351 proteins directly and indirectly regulates actin cytoskeleton dynamics (Chang et al., 2011; Zhao
352 et al., 2013; Tong et al., 2016), a process also influenced by RACB in barley (Opalski et al.,
353 2005). Therefore, it remains conceivable that phosphorylation of these conserved sites may
354 be important for ROP regulation during plant cytoskeleton rearrangement.

355 Using transgenic CA-RACB overexpressing plants, we were able to evidence RACB and
356 higher molecular weight derivatives on a Western blot after proteasome inhibition, which was
357 not observed in the absence of the proteasome inhibitor (compare Fig. 3 and Fig. 5). Since
358 these higher molecular weight derivatives strongly resembled a typical ubiquitination pattern
359 as described for e.g. the plant pattern-recognition receptor flagellin sensing 2 (FLS2) (Gohre
360 et al., 2008; Lu et al., 2011), we excised these bands and investigated RACB ubiquitination via
361 mass spectrometry. This way, we identified RACB K167 as an ubiquitin acceptor site, which is
362 fully conserved across all ROPs of barley, rice and Arabidopsis (see Fig. 6 and Supplemental
363 Figure 3). The respective residue is also ubiquitinated in mammalian Rac1 and Rac3 by the
364 SCF^{FBXL19}-complex, which leads to proteasomal degradation of both proteins (Zhao et al.,
365 2013; Dong et al., 2014). It remains to be elucidated, if comparable regulatory mechanisms
366 are conserved between RHO family proteins across kingdoms.

367 Two other ubiquitination sites present in mammalian RHO proteins are conserved in RACB
368 (see Supplemental Figure 1): K8 and K148. Similar to phosphorylation, ubiquitination of the
369 corresponding sites in RhoA and Rac1 also influences actin cytoskeleton dynamics and
370 associated cellular processes, such as cell motility (Wang et al., 2003; Ozdamar et al., 2005;
371 Torrino et al., 2011; Oberoi et al., 2012; Castillo-Lluva et al., 2013). Cross-kingdom
372 conservation of these sites raises the possibility that they might also be important for the
373 regulation of RACB signaling, but it is not yet known under which conditions these
374 modifications might occur.

375 We previously hypothesized that RACB is regulated similarly to mammalian Rac1.
376 Phosphorylation of Rac1 S71 by AKT leads to SCF^{FBXL19}-mediated ubiquitination at Rac1 K166
377 and subsequent proteasomal degradation, which blocks Rac1 from signaling (Kwon et al.,
378 2000; Chang et al., 2011; Zhao et al., 2013). In plants, activated RACB would be
379 phosphorylated by RBK1 and then targeted for ubiquitination and degradation by an
380 SCF-complex containing SKP1L (Huesmann et al., 2012; Reiner et al., 2016). While we did
381 find ubiquitination at RACB K167 (which corresponds to Rac1 K166, see Supplemental
382 Figure 1), we did not identify RACB S74 as a phosphorylation site. One potential reason for
383 this might be that RBK1 belongs to RLCK class VI_A (Jurca et al., 2008; Huesmann et al.,
384 2012; Reiner et al., 2015), while AKT belongs to the AGC kinases (Rademacher and Offringa,
385 2012). Interestingly, ROPs and AGCs also work together in polar cell development: one
386 AGCVIII kinase, D6PK, binds to specific membrane lipids and cooperates with
387 AtROP2/AtROP6 to form root hairs (Stanislas et al., 2015). Thus far, phosphorylation of ROPs
388 during interaction with AGC kinases has not been described. Hence, it is possible that AGC
389 kinases phosphorylate ROPs, with S74 being one of the potential targets. It could also be that
390 RACB S74 is not the target for a barley SKP1L-containing SCF-complex as hypothesized
391 above. One of the *in vitro* phosphosites in RACB could be alternatively recognized and fulfill
392 this role instead.

393 In Arabidopsis and barley, ROPs and RBK1 or related RLCK VI_A-class kinases seem to have
394 partially opposing biological functions. In previous studies, we have shown that HvRBK1 had
395 the opposite disease phenotype of RACB and negatively regulated its protein stability
396 (Huesmann et al., 2012; Reiner et al., 2016). In Arabidopsis, the ROP-activated RBK1-
397 homolog RLCK VI_A3 is also involved in pathogen resistance rather than susceptibility (Reiner
398 et al., 2015). In Arabidopsis, an auxin-responsive MPK-cascade was associated with AtRBK1
399 (RLCK VI_A4) and ROP signaling. Enders and co-workers could show that *mitogen-activated*
400 *protein kinase kinase kinase 3* (*mkk3), mpk1* and *rbk1* knock-out plants displayed
401 hypersensitivity towards auxin, while *atrop4* and *atrop6* mutants were defective in auxin
402 sensing. Furthermore, they demonstrated that AtROP4 and AtROP6 might be direct

403 phosphorylation targets of AtRBK1 and hypothesized that AtRBK1-mediated phosphorylation
404 negatively influences the activity of both ROPs (Enders et al., 2017). However, this remains to
405 be fully shown, since phosphorylation of His-tagged AtROP4 and AtROP6 was investigated *in*
406 *vitro* and no phosphosites were mapped in this study. Nevertheless, this suggests a general
407 mechanism, in which ROPs are negatively regulated by phosphorylation through RLCK VI_A
408 members in distinct signaling branches.

409 Our data further support that posttranslational lipidation may be important for the signaling
410 ability of RACB. Only full-length CA-RACB increased barley susceptibility towards *Bgh*, while
411 the truncated CA-RACB-ΔCSIL mutant did not (see Fig. 3B). We have shown before that
412 removal of the CaaX-box prenylation motif from RACB results in a shift of CA-RACB's
413 subcellular localization from the plasma membrane to the cytosol and to loss of function in
414 susceptibility (Schultheiss et al., 2003). Importance of the CaaX-box prenylation motif CSIL for
415 RACB function is now confirmed here with stable transgenic plants. We have also reported
416 that the interaction of RACB with its downstream effectors mostly takes place at the plant
417 plasma membrane (Schultheiss et al., 2008; Hoefle et al., 2011; McCollum et al., 2019). It
418 would be interesting to see, if barley ROP effectors can still interact with CA-RACB-ΔCSIL *in*
419 *planta* and localize to the plasma membrane in presence of excessive amounts of cytosolic
420 CA-RACB-ΔCSIL. This could provide another piece of evidence that ROPs need to be plasma
421 membrane-localized to perform their function in signaling and to bind to downstream
422 interactors, as it has been described before (Sorek et al., 2011; Yalovsky, 2015).

423 **Conclusion:**

424 Regulation of RHO family proteins by PTMs has long been established in the animal research
425 field. In plants, however, we are only at the beginning of discovering these regulatory
426 mechanisms of PTMs in ROP signaling. Here, we present the first piece of data on *in vivo*
427 ubiquitination of one ROP from barley. The identified ubiquitination site is conserved in all
428 ROPs from barley, rice and Arabidopsis, and has been described before for mammalian
429 RACB-homologs. This suggests that the lysine residue corresponding to RACB K167 might be

430 a general target for ubiquitination across kingdoms. However, it remains to be elucidated, if
431 the function of this modification is also conserved in plants.

432 **Experimental procedures:**

433 **Heterologous protein expression, purification, and kinase activity measurements**

434 A cDNA clone of CA-*RACB* ((Schultheiss et al., 2003), NCBI GenBank identifier for wildtype
435 RACB: CAC83043.2) was cloned into the bacterial expression vector pET26b out of frame of
436 the N-terminal pelB, but in frame with a C-terminal 6xHIS (Novagen, Merck KGaA, Darmstadt,
437 Germany). This way, no potential artificial phosphorylation site was included (Dorjgotov et al.,
438 2009). The barley protein *RBK1* (NCBI GenBank identifier: HE611049.1) was cloned into the
439 pET28a vector in frame with an N-terminal 6xHIS. Cloning was achieved by restriction-ligation
440 after PCR amplification of the cDNA inserts using *Eco*RI and *Xho*I flanking restriction sites on
441 the C- and N-terminal sequence-specific primers. CA-*RACB* was amplified using
442 RACBCA-EcoRI-F + RACBCA-XhoI-R primers, while both wildtype and kinase-dead *RBK1*
443 were amplified with RBK1-F + RBK1-R primers. The kinase dead (KD, K245D) mutant of *RBK1*
444 was constructed by PCR-mediated site-directed mutagenesis using primers RBK1KD-mut-F +
445 RBK1KD-mut-R. After PCR, the parental DNA was digested with *Dpn*I and the whole reaction
446 was transformed into *E. coli* DH5α cells. Following transformation, plasmids were extracted
447 using a routine Miniprep protocol and checked for mutation by sequencing. All primers can be
448 found in Supplemental Table 3.

449 Proteins were purified using HisSelect Sepharose beads (Sigma-Aldrich, St. Louis, USA) and
450 the *in vitro* kinase reactions were carried out as described earlier (Huesmann et al., 2012;
451 Reiner et al., 2016). Two parallel reactions, one with and one without radioactive γ-^{32}P-ATP
452 were performed with both WT and KD RBK1, using the same amount of RACB-6xHIS as
453 substrate. The amount of the proteins in the reactions was app. 150 pmol of RACB-6xHIS with
454 4 pmol of 6xHis-RBK1-WT or 12 pmol 6xHis-RBK1-KD. The radioactive reaction for
455 autoradiography contained 10 µM of cold ATP and 0.2 MBq γ-^{32}P-ATP, while 100 µM ATP

456 were included in the non-radioactive reaction destined for mass spectrometry analysis. The
457 reactions were terminated after 2.5 h and proteins were separated on 12% SDS-
458 polyacrylamide gels that were stained by Coomassie Brilliant Blue using standard methods.
459 Radioactive gels were dried and exposed to x-ray films. From the non-radioactive gel, the band
460 containing RACB-6xHIS was cut out and sent for phosphosite mapping.

461 To show stability of both WT and KD 6xHis-RBK1, a Western blot was performed according to
462 standard procedures. His-tagged proteins were detected with an anti-polyHistidine−peroxidase
463 antibody (Sigma-Aldrich, St. Louis, USA, A7058).

464 **Bioinformatical analysis**

465 The putative RACB protein fold was built by homology-modelling using SWISS-MODEL
466 (Waterhouse et al., 2018) with AtROP4 (PDB entry: 2NTY.1) as template. The final RACB
467 model contained amino acids 1-178 (from 197 total amino acids). PyMOL V2.3.5 (Schrodinger,
468 2015) was used to generate protein surface structure and cartoon illustrations.

469 All protein sequence alignments were done in Jalview V2.11.0 (Waterhouse et al., 2009) with
470 the MAFFT algorithm running at default settings (Katoh and Toh, 2010). NCBI GenBank
471 identifiers for all aligned proteins are:

472 HvRACB: CAC83043.2; HvRACD: CAD27895.1; HvRAC1: CAD57743.1; HvRAC3:
473 BAJ98596.1; HvROP4: CAD27896.1; HvROP6: CAD27894.1; OsRAC1: XP_015621645.1;
474 OsRAC2: XP_015638759.1; OsRAC3: XP_015625155.1; OsRAC4: XP_015641323.1;
475 OsRAC5: XP_015627011.1; OsRAC6: XP_015625732.1; OsRAC7: XP_015627590.1;
476 AtROP1: NP_190698.1; AtROP2: NP_173437.1; AtROP3: NP_001077910.1; AtROP4:
477 NP_177712.1; AtROP5: NP_195320.1; AtROP6: NP_001190916.1; AtROP9: NP_194624.1;
478 AtROP10: NP_566897.1; AtROP11: NP_201093.1; HsRAC1: NP_001003274.1; HsRHOA:
479 5FR2_A.

480 **Generation of transgenic plants**

481 A full-length cDNA clone of CA-*RACB* (carrying the G15V mutation as described in
482 (Schultheiss et al., 2003)) and CA-*RACB*-ΔCSIL (lacking the last 4 amino acids, but with an
483 artificial stop codon) were amplified by PCR using primers RACBCA-Esp-Start + RACBCA-
484 Esp-Stop and RACBCA-Esp-Start + RACBCA-ΔCSIL-Esp-Stop, respectively. Both constructs
485 were cloned first into pGGEntL-EP12 and subsequently into pGGInAE-226n_35SP_Ntag-
486 3xHA_35ST vectors using procedures adapted from Golden Gate-based cloning (Engler et al.,
487 2008), generating the 3x*HA*-CA-*RACB*(-ΔCSIL) fusion constructs. From these vectors, the
488 CA-*RACB*(-ΔCSIL) fusion constructs were re-amplified by PCR using primers 3xHA-XmaI-F
489 and RACBCA-XmaI-R (3x*HA*-CA-*RACB*) and 3xHA-XmaI-F + RACBCA-ΔCSIL-XmaI-R
490 (3x*HA*-CA-*RACB*-ΔCSIL). The free 3x*HA*-control was amplified using primers 3xHA-XmaI-F +
491 UL1-XmaI-R. All constructs were introduced into pUbifull-AB-M, a derivative of pNOS-AB-M
492 (DNA-Cloning-Service, Hamburg, Germany) with the maize *POLYUBIQUITIN 1* promoter
493 being inserted in the multiple cloning site, by restriction-ligation using *Xma*I. From there, *Sfi*I
494 fragments were transferred into the generic binary vector p6i-2x35S-TE9 (DNA-Cloning-
495 Service, Hamburg, Germany). The binary plasmids were transferred into *A. tumefaciens* strain
496 AGL1 (Lazo et al., 1991) and transgenic plants were generated by agro-inoculation of
497 immature barley embryos according to Hensel et al. (2009). Transgenic plants were identified
498 by *HYGROMYCIN PHOSPHOTRANSFERASE*-specific PCR, which yielded 47 lines for 3xHA-
499 CA-RACB, 37 lines for 3xHA-CA-RACB-ΔCSIL and 40 lines for 3xHA. All lines were
500 propagated under normal growth conditions in the greenhouse. Since all descending lines are
501 segregating in generation T_1, individual plants were screened for transgene integration and
502 expression before use in any experiment. This was achieved using Western blotting detecting
503 the HA-tag (antibody: Anti-HA-Peroxidase, Sigma-Aldrich, St. Louis, USA, 12013819001) and
504 resistance against hygromycin-induced discoloration. For the latter, 7 d old leaves were
505 detached and placed on 0.8% water-agar plates containing 200 µg/ml Hygromycin B (Roth,
506 Karlsruhe, Germany, CP12.2). These plates were put into growth chambers operating under
507 long-day conditions (see below) for roughly 4 d, until discoloration of hygromycin non-resistant
508 plants was observed. All primers can be found in Supplemental Table 4.

509 **Plant and fungal growth conditions**

510 Transgenic barley (*Hordeum vulgare*) plants of spring-type cultivar Golden Promise were
511 grown under long-day conditions (16 h light, 8 h darkness) with a photon flux of at least 150
512 µmol m^{-2} s^{-1} at 18 °C and a relative humidity of 65%. Transgene-expressing plants of
513 generation T_1 were used in all experiments. For protoplast isolation, individual plants of
514 different lines expressing the same construct were pooled. The barley powdery mildew fungus
515 *Blumeria graminis* f.sp. *hordei* race A6 (*Bgh*) was propagated on non-transformed wildtype
516 barley Golden Promise plants under the same growth conditions.

517 **Assessment of *Bgh* penetration efficiency**

518 Primary leaves of transgenic plants were cut and placed on 0.8% water-agar plates. These
519 plates were inoculated with 100-130 spores/mm^2 of *Bgh* and placed under normal growth
520 conditions for 48 h, followed by fixing and destaining leaves in 70% (v/v) ethanol. Fungal
521 spores and appressoria were stained with an ink solution (10% (v/v) Pelikan Ink 4001®
522 (Pelikan, Hannover, Germany), 25% (v/v) acetic acid) and analysed by transmission light
523 microscopy. Haustorium establishment was counted as successful penetration, while stopped
524 fungal growth after appressorium formation was counted as successful plant defense. For each
525 construct (3xHA-CA-RACB, 3xHA-CA-RACB-ΔCSIL and 3xHA), three transgene-expressing
526 plants of one propagated line were analyzed, with at least 96 evaluated plant-fungus interaction
527 sites per plant. Statistical analysis was performed in RStudio V1.2.5033 (source:
528 https://rstudio.com/) using R V3.6.3 (source: https://www.R-project.org). Normal distribution
529 and homogeneity of variance in the penetration assay dataset were confirmed with Shapiro-
530 Wilk's test and Levene's test, respectively. Significant differences of results were assessed
531 using a One-way ANOVA with Tukey's HSD.

532 **Protoplast transformation, proteasome inhibition and protein extraction**

533 Transgenic barley protoplasts stably expressing 3xHA-CA-RACB or 3xHA were isolated and
534 super-transformed as described in Reiner et al. (2016), with the following deviations:

535 transformation reactions were scaled to 1 ml of protoplasts and overnight incubation was
536 conducted in 1 ml buffer WI in single cell culture tubes. For transformation, 50 µg/ reaction of
537 a plasmid coding for *GFP-RBK1* (from Huesmann et al. (2012)) or water (as a mock control)
538 were used. Ten reactions per combination (see Supplemental Figure 2A and B) were prepared.
539 After overnight incubation, MG132 was added to a final concentration of 10 µM, followed by
540 incubation in the dark for 3 h. Protoplasts of corresponding reactions were pooled and pelleted
541 by centrifugation at 120 g. Supernatants were removed and protoplasts were lysed by brief
542 vortexing and snap-freezing in liquid nitrogen. Proteins were resuspended in a modified
543 extraction buffer (10% (w/v) glycerol, 25 mM Tris pH 7.5, 150 mM NaCl, 10 mM DTT, 1 mM
544 PMSF, 1% sodium deoxycholate, 1x protease inhibitor (Sigma-Aldrich, St. Louis, USA, P9599),
545 1 tablet /10 ml PhosSTOP™ (Sigma-Aldrich, St. Louis, USA, 4906845001)) and incubated on
546 ice for 30 min with occasional mixing. This solution was centrifuged at 4 °C to pellet cell debris,
547 the supernatant was digested with trypsin and used in phosphopeptide enrichment (see
548 Supplemental Figure 2A (center panel) and 3B). In one experiment, where the phosphopeptide
549 enrichment was skipped (see Supplemental Figure 2A (bottom panel)), proteins were
550 subjected to immunoprecipitation (see below), loaded on a SDS-PAGE and then submitted to
551 in-gel tryptic digest prior to mass spectrometry. All buffers described in the immunoprecipitation
552 paragraph were used. In another experiment (see Supplemental Figure 2A (top panel)),
553 protoplast lysates were subjected to immunoprecipitation using a modified extraction buffer
554 (10% (w/v) glycerol, 25 mM Tris pH 7.5, 150 mM NaCl, 10 mM DTT, 1 mM PMSF, 50 µM
555 MG132, 1x protease inhibitor (Sigma-Aldrich, St. Louis, USA, P9599), 1 tablet /10 ml
556 PhosSTOP™ (Sigma-Aldrich, St. Louis, USA, 4906845001)) and washing buffer (10% (w/v)
557 glycerol, 25 mM Tris pH 7.5, 150 mM NaCl, 1 mM PMSF, 50 µM MG132, 1x protease inhibitor
558 (Sigma-Aldrich, St. Louis, USA, P9599), 1 tablet /10 ml PhosSTOP™ (Sigma-Aldrich, St.
559 Louis, USA, 4906845001)) and used for on-bead tryptic digest prior to phosphopeptide
560 enrichment via IMAC.

561 **Immunoprecipitation and Western blotting**

562 Transgenic barley leaves expressing 3xHA-CA-RACB or 3xHA were vacuum infiltrated for
563 3 min at -26 mm in Hg with a leaf-floating solution (0.45 M mannitol, 10 mM MES pH 5.7, 10
564 mM $CaCl_2$, 0.0316 g /10 ml Gamborg B5 medium including vitamins (Duchefa, RV Haarlem,
565 The Netherlands, G0210), 50 µM MG132). After incubation in the dark for 3 h, leaves were
566 snap-frozen in liquid nitrogen and homogenized using a TissueLyser II (QIAGEN, Hilden,
567 Germany). Proteins were resuspended in extraction buffer (10% (w/v) glycerol, 25 mM Tris pH
568 7.5, 1 mM EDTA, 150 mM NaCl, 10 mM DTT, 1 mM PMSF, 0.5% Nonidet P40 substitute, 1x
569 protease inhibitor (Sigma-Aldrich, St. Louis, USA, P9599)) by tumbling end-over-end at 4 °C
570 for 30 min. Cell debris was removed by centrifugation and the supernatants were used for
571 immunoprecipitation (IP). IPs were conducted according to routine procedures. Briefly, for
572 each sample, 50 µM Pierce™ Anti-HA Magnetic Beads (Thermo Fisher Scientific, Waltham,
573 USA) were equilibrated 3x in extraction buffer before adding supernatants. HA-tagged proteins
574 were immunoprecipitated by tumbling end-over-end for 1 h at 4 °C, then washed 5x with
575 washing buffer (10% (w/v) glycerol, 25 mM Tris pH 7.5, 1 mM EDTA, 150 mM NaCl, 1 mM
576 PMSF, 1x protease inhibitor (Sigma-Aldrich, St. Louis, USA, P9599)). For selected RACB
577 phosphopeptide screenings (see Supplemental Figure 2A), the beads were directly prepared
578 for mass spectrometry. Otherwise, proteins were eluted in 100 µl of 2x NuPAGE™ LDS
579 Sample Buffer (Thermo Fisher Scientific, Waltham, USA, NP0008) and boiled at 95 °C for 10
580 min. After the IP, 25 µl of eluate were separated on a 12% SDS-PAGE and proteins were
581 transferred to a PVDF membrane. HA-tagged proteins were detected with an
582 Anti-HA-Peroxidase antibody (Sigma-Aldrich, St. Louis, USA, 12013819001). For the RACB
583 ubiquitination screening, the remaining 75 µl were loaded on another 12% SDS-PAGE and
584 silver stained after separation. For this, the SDS-PAGE was incubated in a fixation solution
585 (50% (v/v) methanol, 5% (v/v) acetic acid, 45% (v/v) water) for 1 h and subsequently washed
586 with water three times (two times 2 min each, last time 1 h) on a shaking incubator. The gel
587 was sensitized with a 0.02% (w/v) sodium thiosulfate solution for 2 min, then briefly washed
588 with water twice. Afterwards, the gel was incubated at 4 °C in pre-chilled 0.1% (w/v) silver
589 nitrate for 30 min, then rinsed two times with water for 30 s each. In order to stain proteins, the

590 gel was incubated in a developing solution (0.04% (v/v) formaldehyde in 2% (w/v) sodium
591 carbonate) until a sufficient degree of staining had been obtained. Then, the gel was washed
592 five times in 1% (v/v) acetic acid to stop the reaction. Bands corresponding to 3xHA-CA-RACB
593 and its higher molecular weight derivatives were excised from the gel and the gel slices were
594 prepared for mass spectrometry.

595 **Protein digest and phosphopeptide enrichment**

596 In-gel digestion of SDS-PAGE gel segments was performed according to standard procedures.
597 Briefly, excised gel segments were reduced and alkylated with 10 mM dithiothreitol (DTT) and
598 55 mM chloroacetamide (CAA) followed by digestion with trypsin (Roche). Dried peptides were
599 reconstituted with 0.1% FA in water prior to LC-MS analysis. For peptide retention time
600 monitoring, PROCAL peptide standard (Zolg et al., 2017) was added to peptide mixtures at a
601 concentration of 100 fmol on column.

602 On-bead digestion of one immunoprecipitation sample (from the experiment described in
603 Supplemental Figure 2A (bottom panel)) was performed to facilitate a subsequent
604 phosphopeptide enrichment. Dry beads-bound proteins were incubated with urea buffer (8 M
605 Urea, 50 mM Tris HCl pH 8.5, 10 mM DTT, cOmplete^{TM} EDTA-free protease inhibitor cocktail
606 (PIC) (Roche, Basel, Switzerland, 04693132001), Phosphatase inhibitor (PI-III; in-house,
607 composition resembling Phosphatase inhibitor cocktail 1 (P2850), 2 (P5726) and 3 (P0044)
608 from Sigma-Aldrich, St. Louis, USA) for one hour at 30 °C. The sample was alkylated (55 mM
609 CAA), diluted 1:8 with digestion buffer (50 mM Tris-HCl pH 8.5, 1 mM $CaCl_2$) and pre-digested
610 with trypsin (1:100 protease:protein ratio) for 4 hours followed by overnight digestion with
611 trypsin (1:100 protease:protein ratio) at 37 °C. The sample was acidified to pH 3 with TFA and
612 centrifuged at 14,000 *g* for 15 min at 4°C. The supernatant was desalted on a 50 mg SepPAC
613 column (Waters, Milford, USA; elution buffer 50% acetonitrile, 0.07% TFA).

614 Proteins from protoplast lysates were precipitated overnight with 10% trichloroacetic acid in
615 ice-cold acetone at -20°C. Precipitates were washed two times with ice-cold acetone and dry
616 samples re-suspended in urea buffer (8 M Urea, 50 mM Tris HCl pH 8.5, 1 mM DTT,

617 cOmpleteTM EDTA-free protease inhibitor cocktail (PIC) (Roche, Basel, Switzerland,
618 04693132001), Phosphatase inhibitor (PI-III; in-house, composition resembling Phosphatase
619 inhibitor cocktail 1 (P2850), 2 (P5726) and 3 (P0044) from Sigma-Aldrich, St. Louis, USA).

620 Protein concentration was determined with the Bradford assay (Bradford, 1976). 200 µg
621 (experiment described in Supplemental Figure 2A (center panel)) or 900 µg (all experiments
622 described in Supplemental Figure 2B) total protein was reduced (10 mM DTT), alkylated (55
623 mM CAA), diluted 1:8 with digestion buffer and pre-digested with trypsin (1:100
624 protease:protein ratio) for 4 hours followed by overnight digestion with trypsin (1:100
625 protease:protein ratio) at 37 °C. Samples were acidified to pH 3 with TFA and centrifuged at
626 14,000 *g* for 15 min at 4 °C. Supernatants were desalted on 50 mg SepPAC columns (Waters;
627 elution buffer 50% acetonitrile, 0.07% TFA).

628 Phosphopeptide enrichment was performed using a Fe^{3+}-IMAC column (Propac IMAC-10 4x50
629 mm, Thermo Fisher Scientific, Waltham, USA) as described previously (Ruprecht et al.,
630 2017b). Shortly, desalted peptide samples were adjusted to 30% acetonitrile, 0.07% TFA. For
631 quality control, 1.5 nmol of a synthetic library of phosphopeptides and their corresponding non-
632 phosphorylated counterpart sequence (F1) (Marx et al., 2013), were spiked into samples prior
633 to loading onto the column. The enrichment was performed with buffer A (0.07% TFA,
634 30% acetonitrile) as wash buffer and Buffer B (0.315% NH_4OH) as elution buffer. Collected full
635 proteome and phosphopeptide fractions were vacuum-dried and stored at -80°C until further
636 use.

637 Phosphopeptides from the experiments described in Supplemental Figure 2A (top and center
638 panels) were re-suspended in 50 mM citrate, 0.1% formic acid (FA) and desalted on self-
639 packed StageTips (five disks, Ø 1.5 mm C18 material, 3M Empore™, elution solvent 0.1% FA
640 in 50% ACN). Phosphopeptides from the experiment described in Supplemental Figure 2B
641 were re-suspended in 50 mM citrate, 0.1% formic acid (FA), fractionated on basic reverse
642 phase StageTip microcolumns (five disks, Ø 1.5 mm C18 material, 3M Empore™) and pooled

643 to 4 fractions, as described previously (Ruprecht et al., 2017a). Dried peptides were
644 reconstituted with 0.1% FA in water prior to LC-MS analysis.

645 *In vitro* kinase assay samples were mixed 1:4 with urea buffer (8 M urea, 50 mM Tris-HCl pH
646 7.5). Samples were reduced (5 mM DTT, 1h, room temperature), alkylated (15 mM CAA, 30
647 min, room temperature) and subsequently diluted 1:8 with digestion buffer. In-solution pre-
648 digestion with trypsin (Roche, Basel, Switzerland) was performed for 4 hours at 37 °C (1:50
649 protease:protein ratio), followed by overnight digestion with trypsin (1:50 protease:protein
650 ratio). Samples were acidified to pH 3 using trifluoroacetic acid (TFA) and centrifuged at
651 14,000 *g* for 5 min. The supernatant was desalted on self-packed StageTips (four disks, Ø 1.5
652 mm C18 material, 3M Empore™, elution solvent 0.1% FA in 50% ACN). Dried peptides were
653 reconstituted with 0.1% FA in water prior to LC-MS analysis.

654 **Mass spectrometry**

655 Liquid chromatography-coupled mass spectrometry (LC-MS/MS) analysis was performed on
656 Orbitrap mass spectrometer systems (Thermo Fisher Scientific, Waltham, USA) coupled on-
657 line to a Dionex 3000 HPLC (Thermo Fisher Scientific, Waltham, USA). The liquid
658 chromatography setup consisted of a 75 µm × 2 cm trap column packed in-house with Reprosil
659 Pur ODS-3 5 µm particles (Dr. Maisch GmbH) and a 75 µm × 40 cm analytical column, packed
660 with 3 µm particles of C18 Reprosil Gold 120 (Dr. Maisch GmbH, Ammerbuch, Germany).
661 Peptides were loaded onto the trap column using 0.1% FA in water. Separation of the peptides
662 was performed by using a linear gradient from 4% to 32% ACN with 5% DMSO, 0.1% formic
663 acid in water over 60 min followed by a washing step (70 min total method length) at a flow
664 rate of 300 nl/min and a column temperature of 50 °C. For phosphopeptide fractions, the
665 gradient was adjusted to a two-step gradient from 4% to 27% ACN. The instruments were
666 operated in data-dependent mode, automatically switching between MS and MS2 scans.
667 For the RACB ubiquitination screen samples (see Supplemental Figure 2C), full-scan mass
668 spectra (m/z 360-1300) were acquired in profile mode on a Q Exactive HF with 60,000
669 resolution, an automatic gain control (AGC) target value of 3e6 and 10 ms maximum injection
670 time. For the top 20 precursor ions, high resolution MS2 scans were performed using HCD

671 fragmentation with 25% normalized collision energy, 30,000 resolution, an AGC target value
672 of 2e5, 50 ms maximum injection time and 1.7 *m/z* isolation width in centroid mode. The
673 underfill ratio was set to 1% with a dynamic exclusion of 20 s. To confirm and more precisely
674 monitor the GlyGly- and phospho-modified peptides identified in the global analysis of these
675 samples, a targeted parallel reaction monitoring assay (PRM) was set up on the Q Exactive
676 HF using the same LC gradient settings. Peptide precursor charge states were chosen based
677 on the previous identification results. In addition, a selection of PROCAL retention time
678 calibration mixture peptides was monitored. PRM measurements were performed with the
679 acquisition method switching between experiments after one duty-cycle. The first experiment
680 consisted of a full scan MS1 spectrum recorded in the Orbitrap (360 to 1300 m/z, 15k
681 resolution, AGC target 3e6, Maximum IT 50 ms). The second experiment consisted of a tMS2
682 PRM scan triggering MS2 scans based on a list containing retention time window, m/z and
683 charge information. For the tMS2 PRM scan, the scheduled precursors were isolated (isolation
684 window 1.3 m/z), fragmented via HCD (NCE 25%) and recorded in the Orbitrap (120 to 2,000
685 m/z, 15k resolution, AGC target 2e5, Maximum IT 100 ms).
686 For the kinase assay samples, full scan maximum injection time was 50 ms and MS2 scans
687 were performed with a resolution of 15,000 and 100 ms maximum injection time. His-tagged
688 CA-RACB and RBK1 peptides were set on an inclusion list and the dynamic exclusion set to
689 5s.
690 For the experiments described in Supplemental Figure 2B, full-scan mass spectra (m/z 360-
691 1300) were acquired in profile mode on a Q Exactive HF-X with 60,000 resolution, an automatic
692 gain control (AGC) target value of 3e6 and 45 ms maximum injection time. For the top 20
693 precursor ions, high resolution MS2 scans were performed using HCD fragmentation with 26
694 % normalized collision energy, 30,000 resolution, an AGC target value of 2e5, and 1.3 *m/z*
695 isolation width in centroid mode. The intensity threshold was set to 2.2e4 with a dynamic
696 exclusion of 25 s. RACB and RBK1 peptides were set on an inclusion list. Full proteome
697 samples were measured with 50 ms maximum injection time for MS2 scans, phosphopeptide
698 samples with 100 ms.

699 For the experiment described in Supplemental Figure 2A, full-scan mass spectra (m/z 360-
700 1,300) were acquired in profile mode on an Orbitrap Fusion LUMOS with 60,000 resolution, an
701 automatic gain control (AGC) target value of 4e5 and 50 ms maximum injection time. For the
702 top 15 precursor ions, high resolution MS2 scans were performed using HCD fragmentation
703 with 30% normalized collision energy, 30,000 resolution, an AGC target value of 5e4, 120 ms
704 maximum injection time and 1.7 *m/z* isolation width in centroid mode. The intensity threshold
705 was set to 2.5e4 with a dynamic exclusion of either 27 s (all peptides) or 10 s (RACB peptides
706 set on an inclusion list).
707 Peptide and protein identification and quantification was performed with MaxQuant (Cox and
708 Mann, 2008) using standard settings (version 1.5.8.3). Raw files were searched against a
709 barley database (160517_Hv_IBSC_PGSB_r1_proteins_HighConf_REPR_annotation.fasta;
710 IPK Gatersleben) and common contaminants. For the experiments described in Supplemental
711 Figure 2B, we added the phosphopeptide library sequences (Marx et al., 2013). For the kinase
712 assay dataset, we used the recombinant protein sequences and an *E. coli* reference database
713 (uniprot-proteome_UP000000625). Carbamidomethylated cysteine was set as fixed
714 modification and oxidation of methionine, and N-terminal protein acetylation as variable
715 modifications. Lysine ubiquitylation, phosphorylation of serine, threonine or tyrosine were set
716 as variable modification were applicable. An m/z value of 115.0502 was specified as diagnostic
717 ion for lysine glyglycylation (Zolg et al., 2018). Trypsin/P was specified as the proteolytic
718 enzyme, with up to two missed cleavage sites allowed. The match between run function was
719 enabled for matching samples and between fractions. Results were filtered to 1% PSM, protein
720 and Site FDR. MS spectra were displayed with MaxQuant viewer.
721 RAW files from the PRM measurement of the ubiquitination screen samples were imported
722 into Skyline (64-bit, v.4.1.0.11796) (MacLean et al., 2010) for data filtering and analysis and
723 transition selection was manually refined to include site determining ions for each modification
724 site. Peaks were integrated using the automatic peak finding function followed by manual
725 curation of all peak boundaries and transitions. The summed area under the fragment ion

traces data for every transition was exported for data visualization in Microsoft Excel and used to confirm the expected relative quantity of modified RACB peptides based on the gel segment. The mass spectrometry proteomics data have been deposited to the ProteomeXchange Consortium via the PRIDE (Vizcaíno et al., 2016) partner repository with the dataset identifier PXD019273.

Acknowledgements

We acknowledge the technical assistance of Cornelia Marthe (IPK Gatersleben) in generating the transgenic barley used in this study and Dalma Ménesi for her help with protein purifications (IPB, BRC Szeged). We are grateful to the TUM plant technology center for support in propagation of transgenic barley plants. The contribution of A.F. was supported by a grant from the National Research, Development, and Innovation Office (#K101112; Hungary).

References

Akamatsu, A., Wong, H.L., Fujiwara, M., Okuda, J., Nishide, K., Uno, K., Imai, K., Umemura, K., Kawasaki, T., and Kawano, Y. (2013). An OsCEBiP/OsCERK1-OsRacGEF1-OsRac1 module is an essential early component of chitin-induced rice immunity. Cell host & microbe **13,** 465-476.

Berken, A. (2006). ROPs in the spotlight of plant signal transduction. Cell Mol Life Sci **63,** 2446-2459.

Berken, A., and Wittinghofer, A. (2008). Structure and function of Rho-type molecular switches in plants. Plant Physiol Biochem **46,** 380-393.

Berken, A., Thomas, C., and Wittinghofer, A. (2005). A new family of RhoGEFs activates the Rop molecular switch in plants. Nature **436,** 1176-1180.

Boulter, E., and Garcia-Mata, R. (2010). RhoGDI: A rheostat for the Rho switch. Small GTPases **1,** 65-68.

Bradford, M.M. (1976). A rapid and sensitive method for the quantitation of microgram quantities of protein utilizing the principle of protein-dye binding. Anal Biochem **72,** 248-254.

Castillo-Lluva, S., Tan, C.T., Daugaard, M., Sorensen, P.H., and Malliri, A. (2013). The tumour suppressor HACE1 controls cell migration by regulating Rac1 degradation. Oncogene **32,** 1735-1742.

Chang, F., Lemmon, C., Lietha, D., Eck, M., and Romer, L. (2011). Tyrosine phosphorylation of Rac1: a role in regulation of cell spreading. PLoS One **6,** e28587.

Cox, J., and Mann, M. (2008). MaxQuant enables high peptide identification rates, individualized ppb-range mass accuracies and proteome-wide protein quantification. Nature biotechnology **26,** 1367-1372.

Dong, S., Zhao, J., Wei, J., Bowser, R.K., Khoo, A., Liu, Z., Luketich, J.D., Pennathur, A., Ma, H., and Zhao, Y. (2014). F-box protein complex FBXL19 regulates TGFbeta1-induced E-cadherin down-regulation by mediating Rac3 ubiquitination and degradation. Mol Cancer **13,** 76.

Dorjgotov, D., Jurca, M.E., Fodor-Dunai, C., Szűcs, A., Ötvös, K., Klement, É., Bíró, J., and Fehér, A. (2009). Plant Rho-type (Rop) GTPase-dependent activation of receptor-like cytoplasmic kinases in vitro. FEBS Letters **583,** 1175-1182.

Ebine, K., Fujimoto, M., Okatani, Y., Nishiyama, T., Goh, T., Ito, E., Dainobu, T., Nishitani, A., Uemura, T., Sato, M.H., Thordal-Christensen, H., Tsutsumi, N., Nakano, A., and Ueda, T. (2011). A membrane trafficking pathway regulated by the plant-specific RAB GTPase ARA6. Nat Cell Biol **13,** 853-859.

Ellerbroek, S.M., Wennerberg, K., and Burridge, K. (2003). Serine phosphorylation negatively regulates RhoA in vivo. The Journal of biological chemistry **278,** 19023-19031.

Enders, T.A., Frick, E.M., and Strader, L.C. (2017). An Arabidopsis kinase cascade influences auxin-responsive cell expansion. Plant J **92,** 68-81.

Engelhardt, S., Kopischke, M., Hofer, J., Probst, K., McCollum, C., and Hückelhoven, R. (2019). Barley RIC157 is involved in RACB-mediated susceptibility to powdery mildew. bioRxiv, 848226.

Engler, C., Kandzia, R., and Marillonnet, S. (2008). A one pot, one step, precision cloning method with high throughput capability. PLoS One **3,** e3647.

Fodor-Dunai, C., Fricke, I., Potocky, M., Dorjgotov, D., Domoki, M., Jurca, M.E., Otvos, K., Zarsky, V., Berken, A., and Feher, A. (2011). The phosphomimetic mutation of an evolutionarily conserved serine residue affects the signaling properties of Rho of plants (ROPs). Plant J **66,** 669-679.

Forget, M.-A., Desrosiers, R.R., Gingras, D., and Béliveau, R. (2002). Phosphorylation states of Cdc42 and RhoA regulate their interactions with Rho GDP dissociation inhibitor and their extraction from biological membranes. Biochemical Journal **361,** 243-254.

792 **Gohre, V., Spallek, T., Haweker, H., Mersmann, S., Mentzel, T., Boller, T., de Torres, M.,**
793 **Mansfield, J.W., and Robatzek, S.** (2008). Plant pattern-recognition receptor FLS2 is
794 directed for degradation by the bacterial ubiquitin ligase AvrPtoB. Curr Biol **18,** 1824-
795 1832.
796 **Hensel, G., Kastner, C., Oleszczuk, S., Riechen, J., and Kumlehn, J.** (2009).
797 Agrobacterium-mediated gene transfer to cereal crop plants: current protocols for
798 barley, wheat, triticale, and maize. International journal of plant genomics **2009,**
799 835608.
800 **Hoefle, C., Huesmann, C., Schultheiss, H., Börnke, F., Hensel, G., Kumlehn, J., and**
801 **Hückelhoven, R.** (2011). A barley ROP GTPase ACTIVATING PROTEIN associates
802 with microtubules and regulates entry of the barley powdery mildew fungus into leaf
803 epidermal cells. The Plant Cell **23,** 2422-2439.
804 **Hua, Z., and Vierstra, R.D.** (2011). The cullin-RING ubiquitin-protein ligases. Annu Rev Plant
805 Biol **62,** 299-334.
806 **Huesmann, C., Reiner, T., Hoefle, C., Preuss, J., Jurca, M.E., Domoki, M., Feher, A., and**
807 **Huckelhoven, R.** (2012). Barley ROP binding kinase1 is involved in microtubule
808 organization and in basal penetration resistance to the barley powdery mildew fungus.
809 Plant Physiol **159,** 311-320.
810 **Irani, K., Xia, Y., Zweier, J.L., Sollott, S.J., Der, C.J., Fearon, E.R., Sundaresan, M., Finkel,**
811 **T., and Goldschmidt-Clermont, P.J.** (1997). Mitogenic signaling mediated by
812 oxidants in Ras-transformed fibroblasts. Science **275,** 1649-1652.
813 **Jank, T., Bogdanović, X., Wirth, C., Haaf, E., Spoerner, M., Böhmer, K.E., Steinemann,**
814 **M., Orth, J.H.C., Kalbitzer, H.R., Warscheid, B., Hunte, C., and Aktories, K.** (2013).
815 A bacterial toxin catalyzing tyrosine glycosylation of Rho and deamidation of Gq and
816 Gi proteins. Nature Structural & Molecular Biology **20,** 1273-1280.
817 **Jones, M.A., Shen, J.-J., Fu, Y., Li, H., Yang, Z., and Grierson, C.S.** (2002). The Arabidopsis
818 Rop2 GTPase is a positive regulator of both root hair initiation and tip growth. The Plant
819 Cell **14,** 763-776.
820 **Jurca, M.E., Bottka, S., and Fehér, A.** (2008). Characterization of a family of Arabidopsis
821 receptor-like cytoplasmic kinases (RLCK class VI). Plant Cell Reports **27,** 739-748.
822 **Katoh, K., and Toh, H.** (2010). Parallelization of the MAFFT multiple sequence alignment
823 program. Bioinformatics **26,** 1899-1900.
824 **Klahre, U., and Kost, B.** (2006). Tobacco RhoGTPase ACTIVATING PROTEIN1 Spatially
825 Restricts Signaling of RAC/Rop to the Apex of Pollen Tubes. The Plant Cell **18,** 3033-
826 3046.
827 **Krauthammer, M., Kong, Y., Ha, B.H., Evans, P., Bacchiocchi, A., McCusker, J.P., Cheng,**
828 **E., Davis, M.J., Goh, G., Choi, M., Ariyan, S., Narayan, D., Dutton-Regester, K.,**
829 **Capatana, A., Holman, E.C., Bosenberg, M., Sznol, M., Kluger, H.M., Brash, D.E.,**
830 **Stern, D.F., Materin, M.A., Lo, R.S., Mane, S., Ma, S., Kidd, K.K., Hayward, N.K.,**
831 **Lifton, R.P., Schlessinger, J., Boggon, T.J., and Halaban, R.** (2012). Exome
832 sequencing identifies recurrent somatic RAC1 mutations in melanoma. Nat Genet **44,**
833 1006-1014.
834 **Kwon, T., Chun, J., Kim, J.H., and Kang, S.S.** (2000). Akt protein kinase inhibits Rac1-GTP
835 binding through phosphorylation at serine 71 of Rac1. Journal of Biological Chemistry
836 **275,** 423-428.
837 **Lang, P., Gesbert, F., Delespine-Carmagnat, M., Stancou, R., Pouchelet, M., and**
838 **Bertoglio, J.** (1996). Protein kinase A phosphorylation of RhoA mediates the
839 morphological and functional effects of cyclic AMP in cytotoxic lymphocytes. EMBO J
840 **15,** 510-519.
841 **Lawson, C.D., and Ridley, A.J.** (2018). Rho GTPase signaling complexes in cell migration
842 and invasion. J Cell Biol **217,** 447-457.
843 **Lazo, G.R., Stein, P.A., and Ludwig, R.A.** (1991). A DNA transformation-competent
844 Arabidopsis genomic library in Agrobacterium. Bio/technology (Nature Publishing
845 Company) **9,** 963-967.

Lin, Y., and Yang, Z. (1997). Inhibition of Pollen Tube Elongation by Microinjected Anti-Rop1Ps Antibodies Suggests a Crucial Role for Rho-Type GTPases in the Control of Tip Growth. Plant Cell **9,** 1647-1659.

Lu, D., Lin, W., Gao, X., Wu, S., Cheng, C., Avila, J., Heese, A., Devarenne, T.P., He, P., and Shan, L. (2011). Direct ubiquitination of pattern recognition receptor FLS2 attenuates plant innate immunity. Science **332,** 1439-1442.

MacLean, B., Tomazela, D.M., Shulman, N., Chambers, M., Finney, G.L., Frewen, B., Kern, R., Tabb, D.L., Liebler, D.C., and MacCoss, M.J. (2010). Skyline: an open source document editor for creating and analyzing targeted proteomics experiments. Bioinformatics **26,** 966-968.

Marx, H., Lemeer, S., Schliep, J.E., Matheron, L., Mohammed, S., Cox, J., Mann, M., Heck, A.J., and Kuster, B. (2013). A large synthetic peptide and phosphopeptide reference library for mass spectrometry–based proteomics. Nature biotechnology **31,** 557-564.

McCollum, C., Engelhardt, S., and Hückelhoven, R. (2019). ROP INTERACTIVE PARTNER b interacts with the ROP GTPase RACB and supports fungal penetration into barley epidermal cells. bioRxiv**,** 750265.

Mergner, J., Frejno, M., List, M., Papacek, M., Chen, X., Chaudhary, A., Samaras, P., Richter, S., Shikata, H., Messerer, M., Lang, D., Altmann, S., Cyprys, P., Zolg, D.P., Mathieson, T., Bantscheff, M., Hazarika, R.R., Schmidt, T., Dawid, C., Dunkel, A., Hofmann, T., Sprunck, S., Falter-Braun, P., Johannes, F., Mayer, K.F.X., Jürgens, G., Wilhelm, M., Baumbach, J., Grill, E., Schneitz, K., Schwechheimer, C., and Kuster, B. (2020). Mass-spectrometry-based draft of the Arabidopsis proteome. Nature.

Milburn, M.V., Tong, L., deVos, A.M., Brunger, A., Yamaizumi, Z., Nishimura, S., and Kim, S.H. (1990). Molecular switch for signal transduction: structural differences between active and inactive forms of protooncogenic ras proteins. Science **247,** 939.

Oberoi, T.K., Dogan, T., Hocking, J.C., Scholz, R.-P., Mooz, J., Anderson, C.L., Karreman, C., Meyer zu Heringdorf, D., Schmidt, G., Ruonala, M., Namikawa, K., Harms, G.S., Carpy, A., Macek, B., Köster, R.W., and Rajalingam, K. (2012). IAPs regulate the plasticity of cell migration by directly targeting Rac1 for degradation. EMBO J **31,** 14-28.

Opalski, K.S., Schultheiss, H., Kogel, K.H., and Huckelhoven, R. (2005). The receptor-like MLO protein and the RAC/ROP family G-protein RACB modulate actin reorganization in barley attacked by the biotrophic powdery mildew fungus Blumeria graminis f.sp. hordei. Plant J **41,** 291-303.

Ozdamar, B., Bose, R., Barrios-Rodiles, M., Wang, H.R., Zhang, Y., and Wrana, J.L. (2005). Regulation of the polarity protein Par6 by TGFbeta receptors controls epithelial cell plasticity. Science **307,** 1603-1609.

Pathuri, I.P., Imani, J., Babaeizad, V., Kogel, K.-H., Eichmann, R., and Hückelhoven, R. (2009). Ectopic expression of barley constitutively activated ROPs supports susceptibility to powdery mildew and bacterial wildfire in tobacco. European journal of plant pathology **125,** 317-327.

Pathuri, I.P., Zellerhoff, N., Schaffrath, U., Hensel, G., Kumlehn, J., Kogel, K.H., Eichmann, R., and Huckelhoven, R. (2008). Constitutively activated barley ROPs modulate epidermal cell size, defense reactions and interactions with fungal leaf pathogens. Plant Cell Rep **27,** 1877-1887.

Peng, J., Schwartz, D., Elias, J.E., Thoreen, C.C., Cheng, D., Marsischky, G., Roelofs, J., Finley, D., and Gygi, S.P. (2003). A proteomics approach to understanding protein ubiquitination. Nat Biotechnol **21,** 921-926.

Rademacher, E.H., and Offringa, R. (2012). Evolutionary Adaptations of Plant AGC Kinases: From Light Signaling to Cell Polarity Regulation. Front Plant Sci **3,** 250.

Reiner, T., Hoefle, C., and Hückelhoven, R. (2016). A barley SKP1-like protein controls abundance of the susceptibility factor RACB and influences the interaction of barley with the barley powdery mildew fungus. Molecular plant pathology **17,** 184-195.

Reiner, T., Hoefle, C., Huesmann, C., Ménesi, D., Fehér, A., and Hückelhoven, R. (2015). The Arabidopsis ROP-activated receptor-like cytoplasmic kinase RLCK VI_A3 is

902 involved in control of basal resistance to powdery mildew and trichome branching. Plant
903 Cell Reports **34,** 457-468.
904 **Rolli-Derkinderen, M., Sauzeau, V., Boyer, L., Lemichez, E., Baron, C., Henrion, D.,**
905 **Loirand, G., and Pacaud, P.** (2005). Phosphorylation of serine 188 protects RhoA
906 from ubiquitin/proteasome-mediated degradation in vascular smooth muscle cells.
907 Circulation research **96,** 1152-1160.
908 **Ruprecht, B., Zecha, J., Zolg, D.P., and Kuster, B.** (2017a). High pH Reversed-Phase Micro-
909 Columns for Simple, Sensitive, and Efficient Fractionation of Proteome and (TMT
910 labeled) Phosphoproteome Digests. Methods Mol Biol **1550,** 83-98.
911 **Ruprecht, B., Koch, H., Domasinska, P., Frejno, M., Kuster, B., and Lemeer, S.** (2017b).
912 Optimized Enrichment of Phosphoproteomes by Fe-IMAC Column Chromatography.
913 Methods Mol Biol **1550,** 47-60.
914 **Scheler, B., Schnepf, V., Galgenmuller, C., Ranf, S., and Huckelhoven, R.** (2016). Barley
915 disease susceptibility factor RACB acts in epidermal cell polarity and positioning of the
916 nucleus. J Exp Bot **67,** 3263-3275.
917 **Schrodinger, LLC.** (2015). The PyMOL Molecular Graphics System, Version 1.8.
918 **Schultheiss, H., Dechert, C., Kogel, K.-H., and Hückelhoven, R.** (2002). A small GTP-
919 binding host protein is required for entry of powdery mildew fungus into epidermal cells
920 of barley. Plant Physiology **128,** 1447-1454.
921 **Schultheiss, H., Dechert, C., Kogel, K.H., and Huckelhoven, R.** (2003). Functional analysis
922 of barley RAC/ROP G-protein family members in susceptibility to the powdery mildew
923 fungus. Plant J **36,** 589-601.
924 **Schultheiss, H., Preuss, J., Pircher, T., Eichmann, R., and Huckelhoven, R.** (2008). Barley
925 RIC171 interacts with RACB in planta and supports entry of the powdery mildew
926 fungus. Cell Microbiol **10,** 1815-1826.
927 **Sorek, N., Poraty, L., Sternberg, H., Buriakovsky, E., Bar, E., Lewinsohn, E., and**
928 **Yalovsky, S.** (2017). Corrected and Republished from: Activation Status-Coupled
929 Transient S-Acylation Determines Membrane Partitioning of a Plant Rho-Related
930 GTPase. Molecular and Cellular Biology **37,** e00333-00317.
931 **Sorek, N., Segev, O., Gutman, O., Bar, E., Richter, S., Poraty, L., Hirsch, J.A., Henis, Y.I.,**
932 **Lewinsohn, E., Jürgens, G., and Yalovsky, S.** (2010). An S-Acylation Switch of
933 Conserved G Domain Cysteines Is Required for Polarity Signaling by ROP GTPases.
934 Current Biology **20,** 914-920.
935 **Sorek, N., Gutman, O., Bar, E., Abu-Abied, M., Feng, X., Running, M.P., Lewinsohn, E.,**
936 **Ori, N., Sadot, E., Henis, Y.I., and Yalovsky, S.** (2011). Differential effects of
937 prenylation and s-acylation on type I and II ROPS membrane interaction and function.
938 Plant Physiol **155,** 706-720.
939 **Stanislas, T., Huser, A., Barbosa, I.C., Kiefer, C.S., Brackmann, K., Pietra, S.,**
940 **Gustavsson, A., Zourelidou, M., Schwechheimer, C., and Grebe, M.** (2015).
941 Arabidopsis D6PK is a lipid domain-dependent mediator of root epidermal planar
942 polarity. Nat Plants **1,** 15162.
943 **Tang, J., Ip, J.P.K., Ye, T., Ng, Y.-P., Yung, W.-H., Wu, Z., Fang, W., Fu, A.K.Y., and Ip,**
944 **N.Y.** (2014). Cdk5-Dependent Mst3 Phosphorylation and Activity Regulate Neuronal
945 Migration through RhoA Inhibition. The Journal of Neuroscience **34,** 7425-7436.
946 **Thomas, C., Fricke, I., Scrima, A., Berken, A., and Wittinghofer, A.** (2007). Structural
947 evidence for a common intermediate in small G protein-GEF reactions. Mol Cell **25,**
948 141-149.
949 **Tong, J., Li, L., Ballermann, B., and Wang, Z.** (2013). Phosphorylation of Rac1 T108 by
950 extracellular signal-regulated kinase in response to epidermal growth factor: a novel
951 mechanism to regulate Rac1 function. Mol Cell Biol **33,** 4538-4551.
952 **Tong, J., Li, L., Ballermann, B., and Wang, Z.** (2016). Phosphorylation and Activation of
953 RhoA by ERK in Response to Epidermal Growth Factor Stimulation. PLoS One **11,**
954 e0147103.
955 **Torrino, S., Visvikis, O., Doye, A., Boyer, L., Stefani, C., Munro, P., Bertoglio, J., Gacon,**
956 **G., Mettouchi, A., and Lemichez, E.** (2011). The E3 ubiquitin-ligase HACE1 catalyzes
957 the ubiquitylation of active Rac1. Dev Cell **21,** 959-965.

Vizcaíno, J.A., Csordas, A., Del-Toro, N., Dianes, J.A., Griss, J., Lavidas, I., Mayer, G., Perez-Riverol, Y., Reisinger, F., and Ternent, T. (2016). 2016 update of the PRIDE database and its related tools. Nucleic acids research **44,** D447-D456.

Wang, H.-R., Zhang, Y., Ozdamar, B., Ogunjimi, A.A., Alexandrova, E., Thomsen, G.H., and Wrana, J.L. (2003). Regulation of Cell Polarity and Protrusion Formation by Targeting RhoA for Degradation. Science **302,** 1775-1779.

Waterhouse, A., Bertoni, M., Bienert, S., Studer, G., Tauriello, G., Gumienny, R., Heer, F.T., de Beer, T.A.P., Rempfer, C., and Bordoli, L. (2018). SWISS-MODEL: homology modelling of protein structures and complexes. Nucleic acids research **46,** W296-W303.

Waterhouse, A.M., Procter, J.B., Martin, D.M., Clamp, M., and Barton, G.J. (2009). Jalview Version 2--a multiple sequence alignment editor and analysis workbench. Bioinformatics **25,** 1189-1191.

Wei, J., Mialki, R.K., Dong, S., Khoo, A., Mallampalli, R.K., Zhao, Y., and Zhao, J. (2013). A new mechanism of RhoA ubiquitination and degradation: roles of SCF(FBXL19) E3 ligase and Erk2. Biochimica et biophysica acta **1833,** 2757-2764.

Wennerberg, K., Rossman, K.L., and Der, C.J. (2005). The Ras superfamily at a glance. J Cell Sci **118,** 843-846.

Worby, C.A., Mattoo, S., Kruger, R.P., Corbeil, L.B., Koller, A., Mendez, J.C., Zekarias, B., Lazar, C., and Dixon, J.E. (2009). The fic domain: regulation of cell signaling by adenylylation. Mol Cell **34,** 93-103.

Wu, G., Li, H., and Yang, Z. (2000). Arabidopsis RopGAPs Are a Novel Family of Rho GTPase-Activating Proteins that Require the Cdc42/Rac-Interactive Binding Motif for Rop-Specific GTPase Stimulation. Plant Physiology **124,** 1625-1636.

Yalovsky, S. (2015). Protein lipid modifications and the regulation of ROP GTPase function. J Exp Bot **66,** 1617-1624.

Yang, Z. (2008). Cell polarity signaling in Arabidopsis. Annu Rev Cell Dev Biol **24,** 551-575.

Zhao, J., Mialki, R.K., Wei, J., Coon, T.A., Zou, C., Chen, B.B., Mallampalli, R.K., and Zhao, Y. (2013). SCF E3 ligase F-box protein complex SCFFBXL19 regulates cell migration by mediating Rac1 ubiquitination and degradation. The FASEB Journal **27,** 2611-2619.

Zolg, D.P., Wilhelm, M., Yu, P., Knaute, T., Zerweck, J., Wenschuh, H., Reimer, U., Schnatbaum, K., and Kuster, B. (2017). PROCAL: a set of 40 peptide standards for retention time indexing, column performance monitoring, and collision energy calibration. Proteomics **17,** 1700263.

Zolg, D.P., Wilhelm, M., Schmidt, T., Medard, G., Zerweck, J., Knaute, T., Wenschuh, H., Reimer, U., Schnatbaum, K., and Kuster, B. (2018). ProteomeTools: Systematic characterization of 21 post-translational protein modifications by liquid chromatography tandem mass spectrometry (LC-MS/MS) using synthetic peptides. Molecular & Cellular Proteomics **17,** 1850-1863.

Supplements

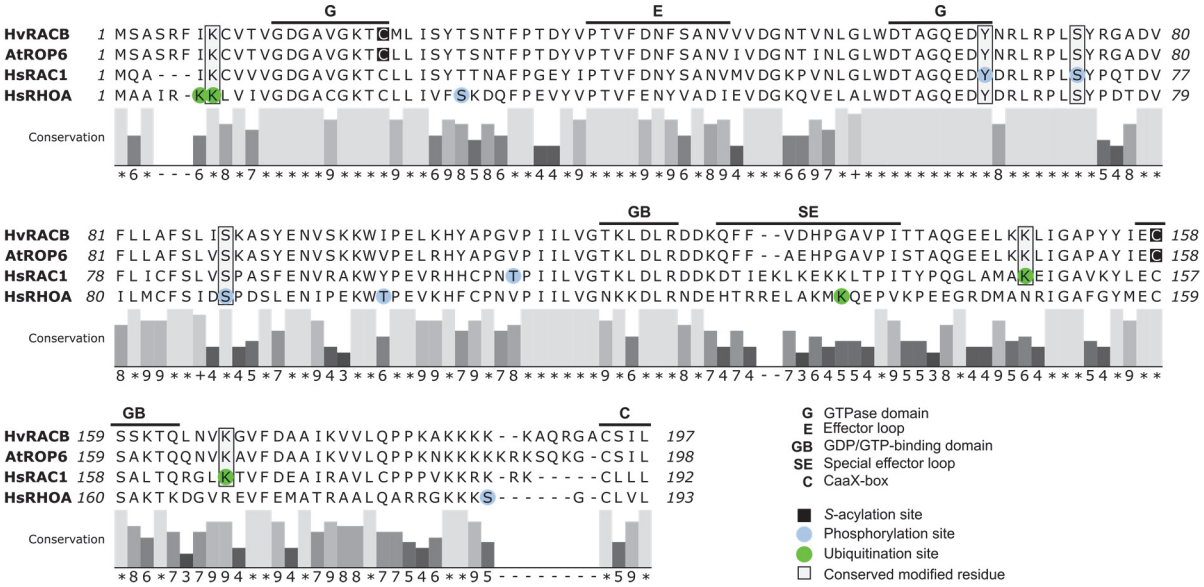

Supplemental Figure 1: Alignment of RACB with AtROP6, HsRAC1 and HsRHOA. Previously published phosphorylation (blue) and ubiquitination (green) sites of mammalian Rac1 and RhoA are highlighted here in the human RAC1 and RHOA sequences. Conserved sites are highlighted in grey boxes. Additionally, the GTPase domain (G), effector loop (E), nucleotide-binding domain (GB), special effector loop (SE) and CaaX-box prenylation motif (C) are illustrated and were taken from Schultheiss et al. (2003). AtROP6 has been shown to be transiently *S*-acylated at two cysteines (Sorek et al., 2010; Sorek et al., 2017), which are also conserved in RACB (black boxes). Conservation of amino acids was determined using MAFFT multiple-sequence alignment in Jalview (Waterhouse et al., 2009; Katoh and Toh, 2010). Conservation scores range from 0 to 11 and are shown as bars (dark grey = less conserved, light grey = highly conserved). Scores of 0, 10, and 11 are shown as "-", "+" and "*", respectively).

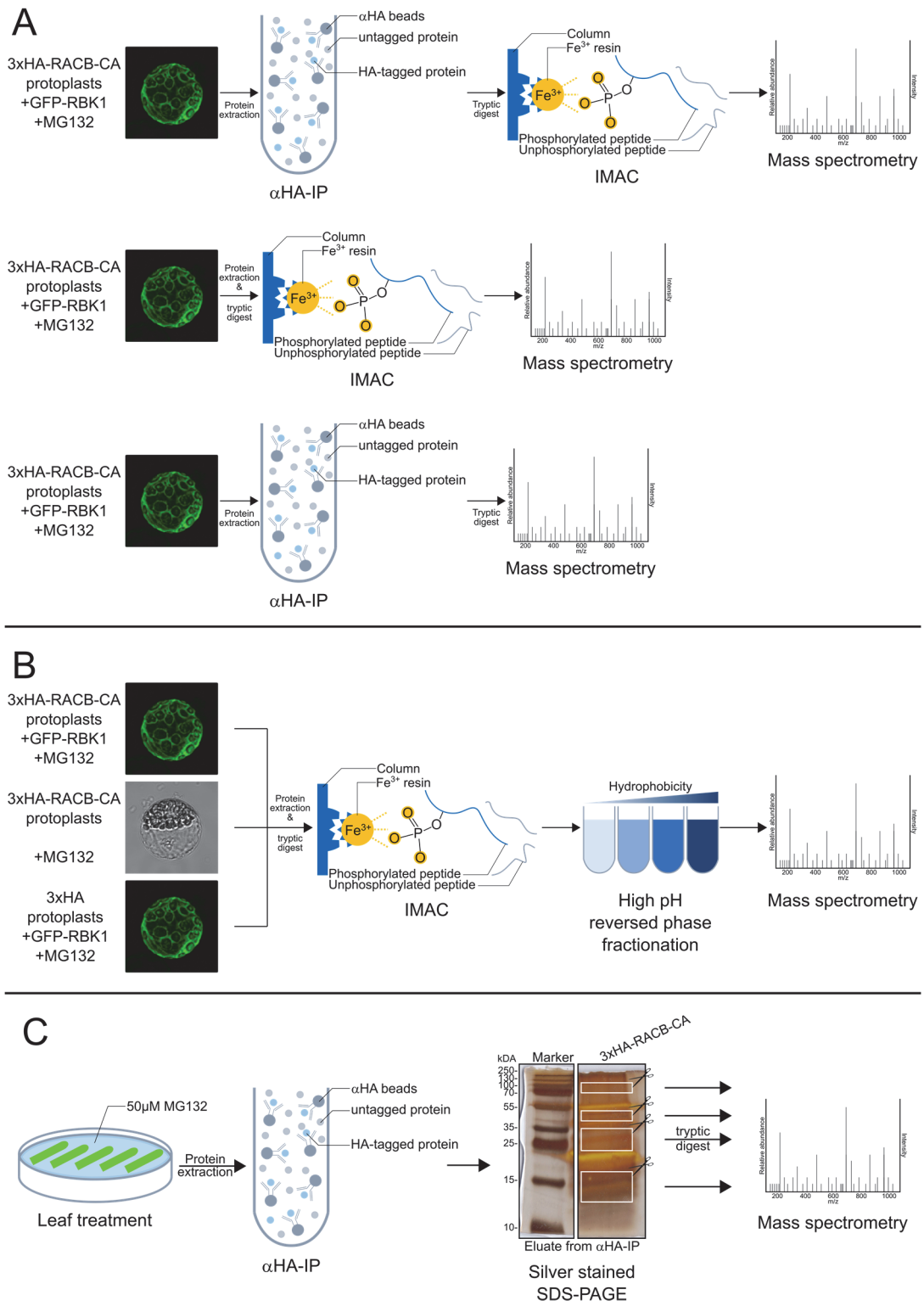

1017

1018 **Supplemental Figure 2: Workflows designed to identify RACB phosphorylation and**

1019 **ubiquitination.**

1020 **A:** Identification of phosphorylated peptides after CA-RACB and RBK1 overexpression.

1021 Protoplasts were isolated from stably transgenic barley leaves overexpressing 3xHA-CA-

1022 RACB. These protoplasts were transiently super-transformed with GFP-RBK1 to stimulate
1023 phosphorylation events of proteins associated with the RACB/RBK1 pathway. After
1024 transformation, all protoplasts were treated with MG132 and proteins were extracted.
1025 HA-tagged proteins were first enriched using immunoprecipitation, followed by tryptic digest
1026 and phosphopeptide enrichment via IMAC (top panel). In two cases, immunoprecipitation or
1027 IMAC were skipped (center and lower panel, respectively). Phosphorylated peptides were
1028 identified using mass spectrometry.

1029 **B:** Second experiment to identify phosphorylated peptides after CA-RACB and/or RBK1
1030 overexpression. Protoplasts were isolated from stably transgenic barley leaves overexpressing
1031 either 3xHA or 3xHA-CA-RACB. These protoplasts were super-transformed with GFP-RBK1.
1032 After transformation, all protoplasts (including an untransformed 3xHA-CA-RACB control) were
1033 treated with MG132. Proteins were extracted and digested with trypsin, followed by enrichment
1034 of phosphopeptides using IMAC. These samples were decomplexed by fractionating the
1035 phosphorylated proteins according to their hydrophobicity. Phosphorylated peptides were
1036 identified by mass spectrometry.

1037 **C:** Analysis of CA-RACB ubiquitination by a targeted approach. Transgenic barley leaves
1038 overexpressing 3xHA-CA-RACB were floated on a solution containing MG132. HA-containing
1039 proteins were enriched by immunoprecipitation and loaded on a SDS-PAGE. Following silver-
1040 staining, RACB-containing bands and those corresponding to the higher molecular weight
1041 derivatives shown in Fig. 5A were excised from the gel (white boxes). After solubilization and
1042 tryptic digest, modification of RACB-peptides was investigated via mass spectrometry.

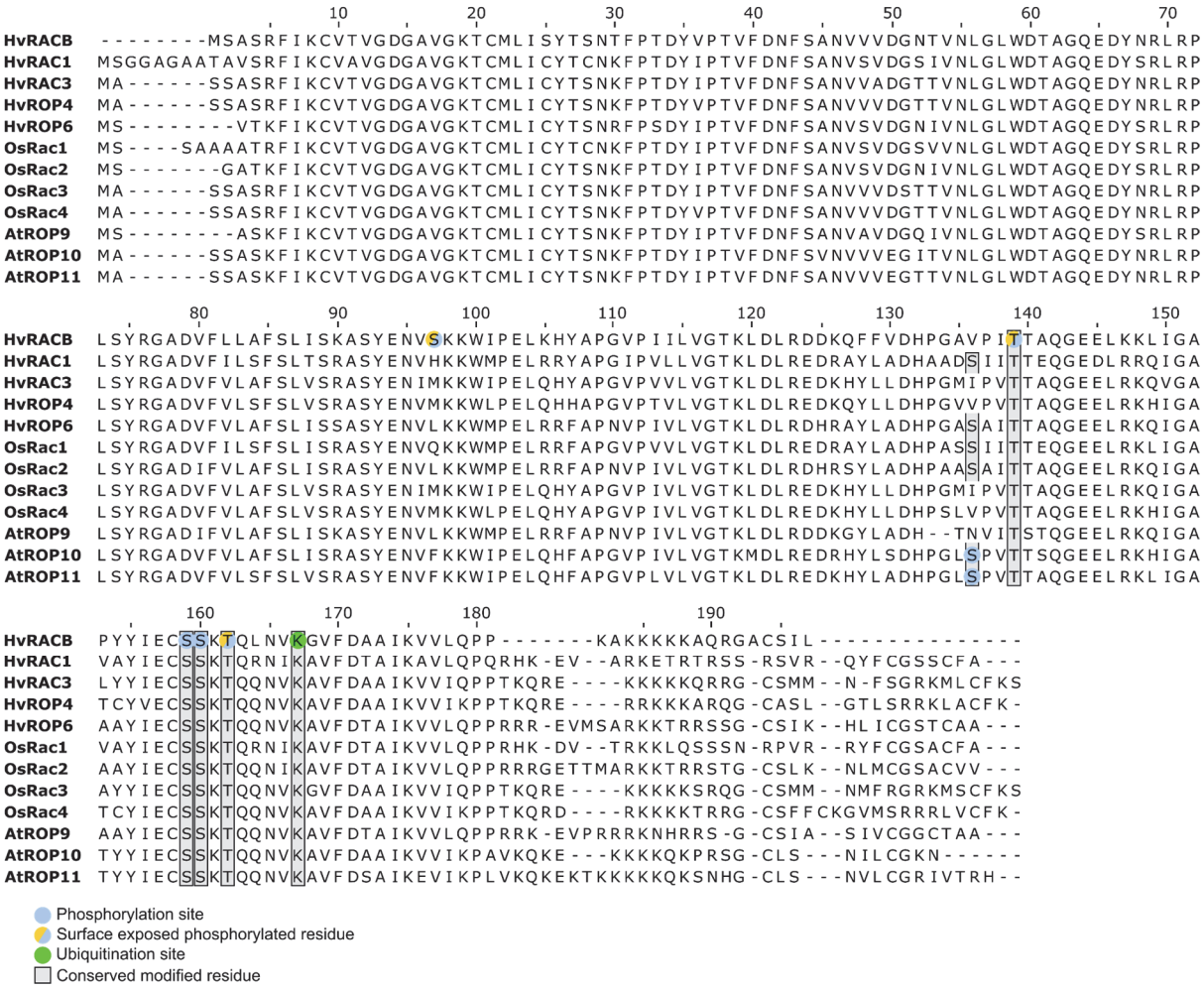

1043

1044 **Supplemental Figure 3: Alignment of barley RACB with type II ROPs from barley, rice**

1045 ***Arabidopsis thaliana*.**

1046 The CA-RACB ubiquitination site at K167 (green) is conserved in all type II ROPs from the

1047 three species (shaded box). *In vitro* phosphorylation sites of RACB (blue) are conserved

1048 among most type II ROPs (shaded box). Surface-exposed phosphosites are additionally

1049 shown in yellow. Conserved of amino acids were identified and aligned using MAFFT multiple-

1050 sequence alignment in Jalview (Waterhouse et al., 2009; Katoh and Toh, 2010).

1051

1052 **Supplemental Table 1:** Dataset of the mass spectrometry analysis of the recombinant RACB
1053 and RBK1 *in vitro* kinase assay.

1054 **Supplemental Table 2:** Dataset containing all identified barley phosphopeptides originating
1055 from transgenic HA-CA-RACB overexpressing protoplasts, which were transformed with
1056 GFP-RBK1 and treated with MG132. HA-tagged proteins and/or phosphopeptides were
1057 enriched by HA-immunoprecipitation and IMAC, respectively (see Supplemental Figure 2A).
1058 All peptides and their modifications were identified by mass spectrometry. Of main interest are
1059 the gene identifiers and peptides with phosphorylated residues and associated localization
1060 scores.

1061 **Supplemental Table 3:** Dataset comprising all recovered barley phosphopeptides from
1062 protoplasts of stable transgenic barley plants. Phosphopeptides were enriched from full-protein
1063 extracts of either HA- or HA-CA-RACB overexpressing protoplasts, which were co-transformed
1064 with GFP-RBK1 and incubated with MG132. Samples were decomplexed by fractionating
1065 phosphopeptides according to their hydrophobicity (see Supplemental Figure 2B). All peptides
1066 and their modifications were identified by mass spectrometry. Non-enriched full-protein
1067 samples (FP) were included in mass spectrometry analyses, but did not yield many
1068 phosphopeptides. Of main interest in this dataset are the gene identifiers and peptides with
1069 phosphorylated amino acids and their corresponding localization scores.

1070 **Supplemental Table 4:** List of all primers used in this study.

1071